Analyses of Spray Atomization Based on Integral Form of Conservation Equations: Applications to Liquid Jets in Cross Flows and to CFD

by

Jung Eun Park

A Thesis Presented in Partial Fulfillment
of the Requirements for the Degree
Master of Science

Approved April 2018 by the
Graduate Supervisory Committee:

Taewoo Lee, Chair
Huei-ping Huang
Kangping Chen

ARIZONA STATE UNIVERSITY

May 2018

ABSTRACT

Liquid injection in cross flows has applications in gas-turbine engines, afterburners and some rocket combustion chambers. Integral form of the conservation equations has been used to find a cubic formula for the drop size in liquid sprays in cross flows. Similar to the work on axial liquid sprays, the energy balance dictates that the initial kinetic energy of the gas and injected liquid be distributed into the final surface tension energy, kinetic energy of the gas and droplets, and viscous dissipation incurred. Kinetic energy of the cross flow is added to the energy balance. Then, only the viscous dissipation term needs to be phenomenologically modelled. The mass and energy balance for the spray flows renders to an expression that relates the drop size to all of the relevant parameters, including the gas- and liquid-phase velocities. The results agree well with experimental data and correlations for the drop size. The solution also provides for drop size-velocity cross-correlation, leading to drop size distributions based on the gas-phase velocity distribution. These aspects can be used in estimating the drop size for practical applications, and also in computational simulations of liquid injection in cross flows, and in other spray geometries in general.

TABLE OF CONTENTS

LIST OF FIGURES

NOMENCLATURE

A	cross-sectional area of the spray in straight flow
A_c	cross-sectional area of the spray in cross flow
A_{inj}	injector exit area
D	drop diameter
D_i	drop diameter for the i-th size bin
D_{32}	SMD, Sauter Mean Diameter, $\sum d_i^3 / \sum d_i^2$
d_{inj}	injector diameter
K, K'	proportionality constants for the viscous dissipation term
n	drop number density
q	momentum flux ratio, $\rho_L u_{inj}^2 / \rho_g u_{in}^2$
u_{inj}	mean injection velocity
u_{in}	velocity of the incoming gas
u_{out}	velocity of the outgoing gas
V	volume of the spray bounded by A and spray length
x_b	distance in the airstream direction
y_m	distance in the direction of liquid injection

z_w spray width

$P(D)$ normalized drop size probability density function

u, u_L mean drop velocity

Greek Symbols

μ_L liquid viscosity

ρ_g ambient gas density

ρ_L liquid density

σ surface tension

$\left\langle \frac{\partial u}{\partial y} \right\rangle$ spatial averaged velocity gradient in the spray

Superscript

$^-$ averaged property

Chapter 1

INTRODUCTION

Determination of the drop size and velocity statistics from sprays is a long-standing problem in two-phase fluid mechanics. From an engineering standpoint, they are important for the obvious reasons of influencing the subsequent vaporization and combustion processes. In practical combustion devices, the fuel is injected in the liquid form and then burned. For this reason, atomization is an integral element in combustion science and engineering. For modeling and computations of spray combustion, the spray drop size and velocities are the starting points [13]. A vast number of works exist in empirical modeling, experimental measurements and computational simulations of drop size and velocity distributions in various spray configurations (a small set of representative works can be found in Ref.[1, 3–5, 8, 9, 13, 14, 25, 31, 34, 37, 41, 43, 45, 46, 48, 51]. More recent work Villermaux and co-workers [33] illustrate the dynamical process during spray atomization including ligament formation and break-up into droplets. Gorokhovski and Herrmann [17] have made advances into resolving detailed structure of atomizing sprays using quasi-DNS; however in that work they also cite the need for simpler, computationally efficient, phenomenological model for realistic Reynolds and Weber number sprays. Some of the models they suggest, such as stochastic scaling, liquid jet depletion, liquid surface density modeling [17], include several components that are currently being investigated for verification and application in spray systems.

Liquid jets in cross flows are of interest in combustion and other spray devices, and much work exists in experimental studies to determine the structure, drop size

and velocity distribution in such flows [12, 15, 21, 22, 42, 49]. In this flow geometry, the gas momentum (and energy) is the main cause for the disintegration and break-up of the injected liquid. This is in contrast to the straight pressure-atomized sprays where it is the liquid momentum (kinetic energy) that is the dominant driver of the subsequent atomization process. Liquid streaming into cross flows has important applications in gas-turbine engine combustion such as afterburners, low NOx burners, high-speed combustors (e.g. supersonic combustors), and also in cooling sprays for turbine blades and in rocket engine combustion. Recent works on liquid atomization in cross flows focus on gas-turbine applications [6, 18, 20, 36]. As the fuel is injected in gas-turbine combustors in a swirl pattern at some angle with respect to high-speed incoming air, liquid jets in cross flows can be considered as a baseline geometry for more complex fuel injection in gas-turbine combustors.

Recently, a new alternate framework for calculating the drop size distribution and velocities based on the integral form of the conservation equations of mass, momentum and energy was presented [24, 26, 27]. In this approach, the conservation equations for spray flows, after some algebraic work, render themselves solvable through iterative methods. The key is to use the integral form of the conservation equations so that the input injection parameters are related to the output spray parameters, without having to resolve the details of the atomization physics. This is a departure from existing methods, where conservation laws are applied in an integral form between "asymptotic" states, therefore bypassing the need for detailed modeling nor complex set of assumptions. Validations of the solutions have been provided in previous works [24, 26, 27], and this method is viable in solving for the drop size and velocities in different spray configurations. Both the mean drop and size distributions, obtained using the current method, agree well with experimental data [26]. The only main

assumption in this formulation is that the liquid phase completes the transition from its initial state to a final state of fully-atomized group of spherical droplets within the specified control volume, and that the viscous dissipation can be written in terms of known parameters such as the liquid velocity and dissipation length scale.

Lefebvre [28] had used a simple zero-dimensional relationship where the kinetic energy of the atomizing air is equated with the final surface tension energy. The rest of the energy terms and their effects are lumped into a parameter representing the efficiency of the atomizing process, so there are only two terms in this energy relationship and no viscous term. Therefore, as the title of that work ("Energy considerations in twin-fluid atomization [29]") indicates, it is a zero-dimensional energy consideration, not a full energy balance in a control volume setting. The current formulation is a complete set of mass, energy (and momentum), where the momentum balance has also been used in some of our previous work for a complete solution of the spray atomization problem [23, 24, 26, 27].

The current approach as in the past work [23, 24, 26, 27] avoids any *ad-hoc* modeling or assumptions and uses the conservation laws in integral (enveloping control volume) sense. Some correlations based on experimental data exist (e.g. [19, 22, 30]) for liquid sprays in cross flows; however, as noted at the outset some of these correlations only provide the primary break-up drop size. Also, due to a large number of parameters, it is difficult to run experiments to come up with a general correlation that incorporates and validates the effects of all the relevant variables. Current analysis and results can synthesize the existing data and can be extended to other fluids and spray conditions, since they are based on fundamentally correct physics of spray atomization (conservation laws). Thus, the current approach represents a

viable method for dealing with this complex spray atomization process and bears both practical and fundamental significance.

The trajectories of the liquid as a function of the so-called momentum ratio ($q = \rho_L u_{inj}^2 / \rho_g u_{in}^2$) are well characterized, and there appear to be reasonable agreements between different experimental results [12, 22, 49]. Faeth and co-workers [22] measure the drop size close to the curved liquid column, naming such drop formation process as the primary atomization. Subsequent "secondary" atomization then is still undetermined, at least not measured in their study [22]. Other studies present plots the Sauter mean diameter (SMD) as a function of the coordinates following the liquid trajectory, or at some arbitrary, fixed location downstream [22]. Unless the gas velocity is extremely high, the liquid and gas interact over a distance to produce droplets of varying size, which typically decreases as the distance from the injection point increases. The interaction of the gas and liquid continues, and the asymptotic final drop size is not always evident [13, 14, 37]. The "atomization length" in the gas streamwise direction will vary as a function of the flow conditions, results in a large test section required to capture this full atomization process. A few studies do present data for practical use toward gas-turbine applications, where the average drop size is measured for the entire plane downstream of the liquid column [6, 15, 36, 42]. Recent experimental data by Freitag and Hassa [15] and others [21, 42] are compared with the cubic formula to investigate validation of the current theory later in this paper.

There are a few experimental correlations for the drop size [6, 15, 19, 22], but they tend to be limited in their scope. As noted above, Faeth and co-workers [22] only report the primary break-up drop size near the liquid core where the drop size increases as a function of the streamwise direction along the liquid column. A general correlation is presented in an earlier work by Ingebo [19], where the SMD is correlated

with the product of Weber and Reynolds numbers. These correlations may be useful at high Weber numbers (large gas velocities), but they yield finite drop size even when the gas velocity is close to zero. Thus, a need exists for a theoretical basis for putting together the experimental results. Other structural data can also be found [2, 11, 16, 32, 35], where various effects on the fluid dynamic aspects of the liquid jets in cross flows are revealed. In particular, Eriksson [11] uses particle image velocimetry (PIV) and phase Doppler anemometry to determine the gas-and liquid-phase velocities, and the drop size. In spite of these sets of data, a theoretical formulation that encompasses all the relevant parameters would be quite useful in bringing the physical variables together in a fluid-dynamically sensible manner. Such a formulation can then be used across a wide range of conditions, based on available data.

Chapter 2

MATHEMATICAL FORMULATION

2.1 Sprays with quiescent surrounding gas

The basic integral form of the conservation equations for mass, momentum and energy has been shown in previous work [24, 26, 27]. Here, we reiterate the formulation for general use. A control volume is considered that envelops the spray including all its complex break-up and atomization mechanisms, as shown in Fig.1.

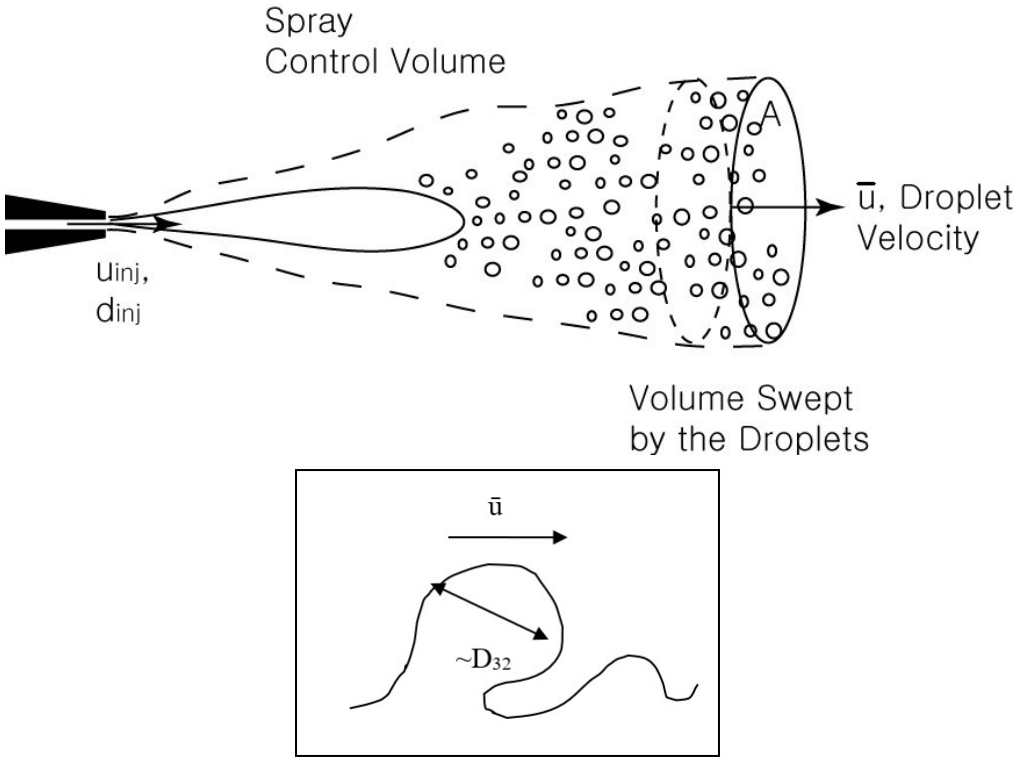

Figure 1. The schematic of the spray control volume used for the integral analysis
Note: The inset shows the reasoning for the viscous dissipation term in Eq.(5).

The approach is to relate the mass, momentum and energy of the spray at the injector exit, to those at a downstream location where the spray is fully atomized. Thus, it enables to avoid the treatment of the complex atomization physics in which expressed in partial differential equations, and to attempt to find an "integral" relationship between the asymptotic states. Heat and mass transfer effects are not yet included, although it is not a far stretch of the current method to include them.

For the control volume described above, the integral form of conservation equations of mass and energy for the liquid phase are as follows:

$$\rho_L u_{inj} A_{inj} = \int_{u=0}^{u_{max}} \int_{D=0}^{D_{max}} n\overline{p}(D,u)\frac{\pi D^3}{6}\rho_L u A \mathrm{dDdu} \approx \frac{\pi}{6} n \rho_L \overline{u} A \sum_i^N P(D_i) D_i^3 \Delta D_i \tag{1}$$

$$\rho_L \frac{u_{inj}^3}{2} A_{inj} = \frac{\pi}{12} n \rho_L \overline{u}^3 A \sum_i^N P(D_i) D_i^3 \Delta D_i + n\overline{u} A \pi \sigma \sum_i^N P(D_i) D_i^2 \Delta D_i + K \mu_L \left\langle \left(\frac{\partial u}{\partial y} \right)^2 \right\rangle (Vol) \tag{2}$$

The mass conservation is achieved by equating the injected mass flow rate with the mass of the droplets contained in a volume swept by the average drop velocity, $\overline{u}$, over a spray area, A. The velocity distribution is simplified to an average drop velocity in Eqs.(1) and (2). This formulation becomes yet simpler for a fixed droplet diameter, which would allow for a transform of velocity to drop size distributions, as will be shown later. The cross-sectional area, A, represents the physical extent of the spray at the plane where full atomization is achieved, which can be determined by the spray cone angle and the atomization length. The drop number density is n, while ρ_L and D_i are the liquid density and droplet diameter, respectively. $P(D_i)$ is

the normalized drop size distribution, and ΔD_i the drop size bin width. The liquid- and gas-phase momentum equations can be included in iterative numerical solutions [24, 26, 27], which would involve the drop drag coefficient and effects of density of both gas (in the drag term) and liquid (in the momentum term). Such momentum effects have been discussed in length in one of previous work [24]. Here, we focus on the SMD-velocity relationship, by using the mass Eq.(1) and energy balance Eq.(2). An estimate of the average viscous dissipation can be written as follows:

$$\mu_L \left\langle \left(\frac{\partial u}{\partial y} \right)^2 \right\rangle \textit{(Spray Volume)} \sim \mu_L \left(\frac{\overline{u}}{D_{32}} \right)^2 \textit{(Spray Volume)} \tag{3}$$

Physically, the deformation of the spray liquid column toward droplets would occur at some velocity scale which will be employed as a mean liquid velocity, and at the length scale of the droplets formed. The length scale is taken to be the SMD itself, since that is the scale at which the liquid deformation leading to droplet formation occurs, as depicted in Fig.1 inset. K is the only adjustable constant in this formulation, as the exact relationship between the viscous dissipation terms and the spray volume is approximated. The dissipation term in previous work [24, 26, 27] was only dimensionally correct, and *ad-hoc*. It led to some reasonable results, but also caused some numerical difficulties when the liquid velocity was large or close to the injection velocity. Clearly, the reason for this previous numerical instability is evident since as shown below when the liquid velocity approaches the injection velocity, the expected drop diameter is infinite (see Fig.3, for example). Schmehl [40] notes that for droplet breakup (secondary atomization) processes the droplet viscous dissipation is exactly $16\pi\mu R_o^3 \left(\dot{y}/y\right)^2$, where R_o is the initial drop radius, y the ellipsoid coordinate

and therefore dy/dt the surface velocity. Eq.(3) is mathematically analogous to the expression of Schmehl [40], where the ratio of the velocity to dissipation length scale is squared and then multiplied by a volume term.

In order to obtain specific equation for D_{32}-velocity relationship, the drop number density, n, is derived from Eq.(1);

$$n = \frac{\rho_L u_{inj} A_{inj}}{\frac{\pi}{6}\rho_L \overline{u} A \sum_{i}^{N} P(D_i) D_i^3 \Delta D_i} \tag{4}$$

Subsequently, substitution of both Eq.(3) and (4) into the energy equation (Eq.(2)) gives us a quadratic equation (Eq.(5)) for the D_{32}. K' now absorbs the spray volume term, for simplicity. As will be discussed later (in Figures 7 and 8), K' increases with increasing distance from the injector, as the spray volume increases.

$$\rho_L \left(\frac{u_{inj}^2 - \overline{u}^2}{2} \right) D_{32}^2 - 6\sigma D_{32} - K' \mu \overline{u}^2 = 0 \tag{5}$$

Lastly, a quadratic solution for the D32 is determined using simple algebra in Eq.(6). The branch with the negative sign (before the square-root term) is discarded, due to its non-physical value. This is an expression for the closed-form solution for the drop size-velociy relation in pressure-atomized sprays, named "quadratic formula".

$$D_{32} = \frac{3\sigma + \sqrt{9\sigma^2 + K' \rho_L \mu \overline{u}^2 \frac{u_{inj}^2 - \overline{u}^2}{2}}}{\rho_L \frac{u_{inj}^2 - \overline{u}^2}{2}} \tag{6}$$

The "quadratic formula" gives accurate predictions for the drop size when compared with experimental and correlation results [23]. Earlier work from this laboratory also suggest general applications of this method, and agreements with experimental and correlation data are quite good [24, 26, 27]. For liquid sprays in cross flows, it is

mostly the gas- phase momentum and kinetic energy that cause the break-up of the liquid column and subsequent atomization. This fact drives to try a broaden application along basic concept of energy conservation using integral form which easily be incorporated in the previous work.

2.2 Sprays in cross flows

Relative motion between the liquid and the gas causes the disruption, eventual break-up and atomization of the liquid. Good correlations exist for the liquid jet penetration and trajectories in other paper [12, 22, 49] conducted for a wide range of conditions. In this study, to resolve the effect of gas-phase velocities, liquid injection and other parameters are considered on the final drop size. As noted earlier, this approach involves direct, robust applications of the conservation laws for mass and energy in integral form [24, 26, 27]. Momentum balance can be included to develop relationships between the liquid- and gas-phase velocities, for which iterative solutions are possible [24].

A control volume is schematically drawn in Fig.2, which has the cross-sectional area, A_c, described later with Eq.(7) and (8). Liquid is injected vertically into gas flowing left to right, perpendicular to the liquid jet. Specifically, liquid injection is considered to being perpendicular to the airflow direction, although any injection angle relative to the cross flow can potentially be analyzed using trigonometric relations. The liquid column is bent and one can experimentally observe the break-up near the surface extending downstream [12, 15, 22, 49]. Subsequently, downstream from the location where the tip of the liquid column is completely depleted, the spray flow evolves to a dilute field of droplets. The control volume extends close to the wall in

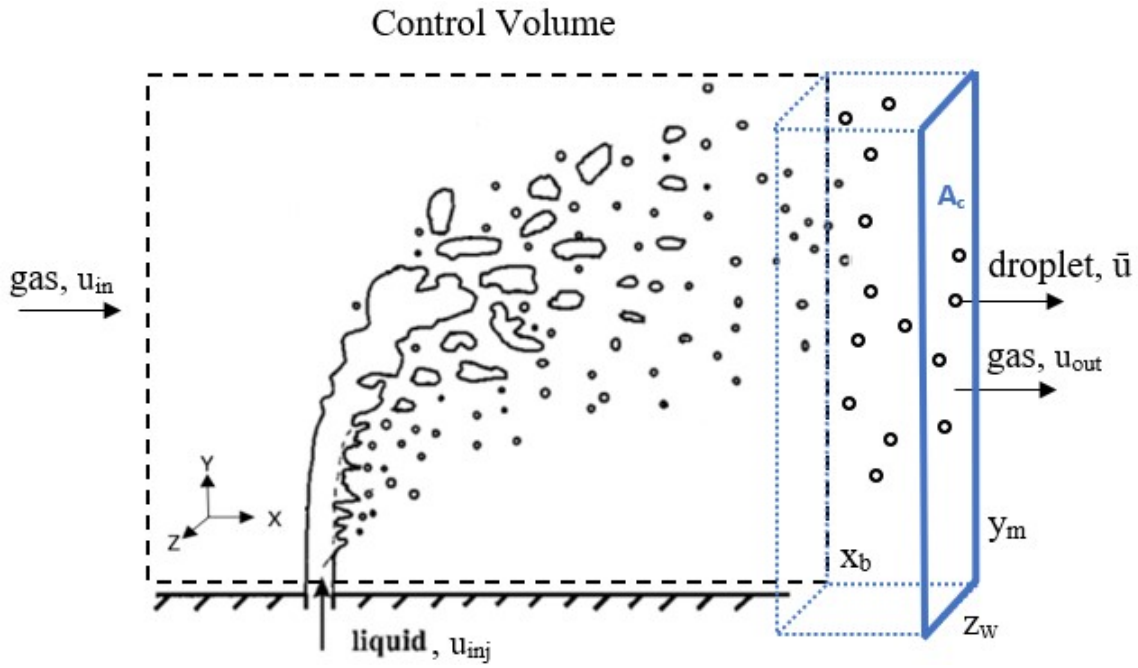

Figure 2. Basic geometry for the liquid jet atomization in a cross flow

this geometry since the flow is parallel to the wall, droplet trajectories also become parallel near the wall. The end of the control volume is designated at a downstream position where the break-up process has been completed. At this plane, there would exist a momentum and energy equilibrium, with some liquid, $\overline{u}$, and gas velocity, u_{out}, at this plane. The plane has the cross-sectional area, A_c, proportional to the initial liquid column cross sectional area. There are several examples of good data on u_{out} as the velocities can be measured using PIV or laser/phase Doppler anemometry [2, 6, 11, 12, 15, 22, 32, 49]. To quantify the mass, momentum and energy of interest, those concepts play a role of constructing integral form of equation efficiently in this paper.

A_c is the cross-sectional area of the control volume enveloping the spray and can be estimated from the liquid jet penetration, y_m, and width z_w. For example, Wu et al. [49] have performed extensive measurements of the liquid jet geometry, and the following often-cited correlations can be used to estimate $A_c = z_w y_m$, where

$x = x_b =$ (column fracture point) $= 8.06 d_{inj}$. q is the momentum ratio in Eqs. (7) and (8) [49].

$$\frac{z_w}{d_{inj}} = 4.3 q^{0.33} \left(\frac{x}{d_{inj}} \right)^{0.33} \tag{7}$$

$$\frac{y_m}{d_{inj}} = 7.86 q^{0.17} \left(\frac{x}{d_{inj}} \right)^{0.33} \tag{8}$$

For the cross flow, the integral form for the mass and energy balance in the control volume described above as follows:

$$\rho_L u_{inj} A_{inj} = \int_{u=0}^{u_{max}} \int_{D=0}^{D_{max}} n \overline{p}(D,u) \frac{\pi D^3}{6} \rho_L u_L A_c dD du \approx \frac{\pi}{6} n \rho_L \overline{u}_L A_c \sum_i^N P(D_i) D_i^3 \Delta D_i \tag{9}$$

$$\rho_L \frac{u_{inj}^3}{2} A_{inj} + \rho_g \frac{u_{in}^3}{2} A_c = \frac{\pi}{12} n \rho_L \overline{u}_L^3 A_c \sum_i^N P(D_i) D_i^3 \Delta D_i + n \overline{u}_L A_c \pi \sigma \sum_i^N P(D_i) D_i^2 \Delta D_i + K \mu_L \left\langle \left(\frac{\partial u_L}{\partial y} \right)^2 \right\rangle (Vol) + \rho_g \frac{u_{out}^3}{2} A_c \tag{10}$$

Eq.(9) is a straight-forward mass balance between the injected fluid and the droplet mass flow rate. For the energy balance, it has been added that the gas-phase kinetic energy entering and leaving the control volume, as parameterized by u_{in} and u_{out}, respectively. The input energy is the kinetic energy of the liquid and gas, which is distributed into the droplet kinetic energy, surface tension energy, viscous dissipation, and gas kinetic energy in Eq.(10). As in our previous work, this integral formulation bypasses the complex physics, and relates the input and output terms. Also, it is reasonable to write the viscous dissipation term as [23]:

$$K\mu_L \left\langle \left(\frac{\partial u_{_L}}{\partial y} \right)^2 \right\rangle \textit{(Spray Volume)} \sim K'\mu_L \left(\frac{\overline{u}_{_L}}{D_{32}} \right)^2 \tag{11}$$

The viscous term includes the spray volume, to be consistent with the rest of the terms in Eq.(10). The above phenomenological expression for the viscous dissipation means that on the average the shear stress of the droplet tearing from the liquid surface occurs at the velocity and length scales of the mean liquid velocity and mean drop size, respectively. The liquid is strained by velocity $\overline{u}_L$, and the length scale over which this strain occurs on the average can be written as D_{32}. Schmehl [40] notes that for droplet breakup during secondary atomization the droplet viscous dissipation is $16\pi R_o^3 \left(\frac{\dot{y}}{y}\right)^2$, where R_o is the initial drop radius, y the ellipsoid coordinate and therefore dy/dt the surface velocity. Eq.(11) is mathematically analogous to the expression by Schmehl [40], as was done for straight flows.

It is not surprising from the fact of that the way to identify a specific equation for the D_{32}-velocity relationship in cross flow is quite similar to the previous procedure in straight airflow, since it characterizes in the respect of being based on the fundamental physics law. Similar to the previous case, n, is directly computed from Eq.(9).

$$n = \frac{\rho_L u_{inj} A_{inj}}{\frac{\pi}{6}\rho_{_L}\overline{u}_{_L} A_c \sum_i^N P(D_i) D_i^3 \Delta D_i} \tag{12}$$

Secondly, substitution of Eqs. (11) and (12) into Eq.(10) again results in the quadratic equation for D_{32}. It is the following Eq.(13):

$$\left[\frac{\rho_L u_{inj}^2}{2}\left(1-\left(\frac{\overline{u}_L}{u_{inj}}\right)^2\right)+\frac{u_{in}A_c}{u_{inj}A_{inj}}\frac{\rho_g u_{in}^2}{2}\left(1-\left(\frac{u_{out}}{u_{in}}\right)^3\right)\right]D_{32}^2$$
$$-6\sigma D_{32}-\frac{K'\mu_L}{u_{inj}A_{inj}}\overline{u}_L^2=0 \quad (13)$$

Finally, the positive branch of the quadratic solution for D32 calculated from Eq.(13) is taken, because it is physically meaningful whereas negative one is not. Solution form for the D_{32} is presented as follows :

$$D_{32}=\frac{3\sigma+\sqrt{9\sigma^2+\frac{K'\mu_L\overline{u}_L^2}{u_{inj}A_{inj}}\left[\frac{\rho_L u_{inj}^2}{2}\left(1-\left(\frac{\overline{u}_L}{u_{inj}}\right)^2\right)+\frac{u_{in}A_c}{u_{inj}A_{inj}}\frac{\rho_g u_{in}^2}{2}\left(1-\left(\frac{u_{out}}{u_{in}}\right)^3\right)\right]}}{\left[\frac{\rho_L u_{inj}^2}{2}\left(1-\left(\frac{\overline{u}_L}{u_{inj}}\right)^2\right)+\frac{u_{in}A_c}{u_{inj}A_{inj}}\frac{\rho_g u_{in}^2}{2}\left(1-\left(\frac{u_{out}}{u_{in}}\right)^3\right)\right]} \quad (14)$$

Although Eq.(14) has been obtained from a quadratic equation, we refer to it as a "cubic formula" due to the significance of the gas velocity ratio term, which is cubed. Later (Fig.6), it is shown that the drop size indeed follows a cubic curve, as a function of the outgoing gas velocity (u_{out}).

Comparing Eqs. (6) (straight) and (14) (cross-flow), we can see that the gas-phase kinetic energy term dominates the cross-flow atomization for $u_{in} \sim 100m/s$ and above. The liquid injection velocities are typically small during cross-flow injections, compared to the gas-phase velocity which is relatively appreciably high [6, 12, 15, 20–22, 36, 42, 49]. Therefore, it is sufficient to postulate that the kinetic energy flow rate is nearly proportional to the cube of the initial gas velocity and this term can overwhelm

the liquid phase kinetic energy for typical momentum ratios. The energy balance (Eq.(13)) and its solution (Eq.(14)) show that it is the retardation of the gas-phase kinetic energy due to aerodynamic interaction with the liquid-phase that tend to dictate the final drop size. The surface tension energy and viscous dissipation affect the final energy balance as well, and these effects are typically parameterized through the Weber (surface tension effect) and the Reynolds (viscosity) number. Eq.(14) is somewhat lengthy but has only three variable parameters to determine $D_{32}; K', \overline{u}_L$ and u_{out}. Of these, only K' is truly adjustable parameter, as $\overline{u}_L$ and u_{out} are the mean droplet and outgoing gas velocities, respectively. They will be related to one another through the momentum equation, and approximate values can also be computed iteratively similar to our work in [23, 24, 26]. In that work, momentum balance for the gas- and liquid- phase provided two additional equations to relate u_{out} to u_{in} and $\overline{u}_L$ to u_{inj}, which came from earlier researcher (Rothe and Block, 1977). Geometric shape of droplets in atomization was assumed as a spherical in this expression.

$$\rho_g u_{in} A_c + \rho_L u_{inj} A_{inj} = \rho_L \overline{u}_L A_c + \rho_g u_{out} A_c$$

$$\frac{\pi}{6} D_{32} \rho_L \overline{u}_L \frac{d\,\overline{u}_L}{dx} = -C_D \frac{\pi}{4} D_{32}^2 \rho_g \frac{(\overline{u}_L - u_{out})^2}{2}$$

Also, integration to CFD is possible by using the computed velocities to find the initial estimates of the drop size, and iterating until computed velocities and drop size (calculated using Eq.(11)) become mutually consistent [24, 26]. In Eqs. (10) and (11), the parameter K' prescribes the average viscous dissipation in the control volume, and it has the spray volume term in it [23]. In Fig.2, the control volume is

drawn to envelop the entire spray, where the average velocities at the inlet and exit are used in Eq.(14). However, as in previous study [23], localized control volumes can be drawn (e.g. horizontal strips) in Fiq.2. Then, local velocities can be used in Eq.(14) to find spatial distribution of D_{32}. For experimental data, this would require spatially-resolved velocity data. For computational simulations, local velocities can be used for estimation of the drop size at specific locations. Some examples of this application to computational simulations will be discussed in Chapter 4, similar to a previous work [23].

Chapter 3

RESULTS AND DISCUSSION

The previous results in this laboratory for straight spray flows with and without swirl [23] are first presented, where the SMD calculated using the quadratic formula showed good agreement and physical trends, when compared with experimental observations. The key formulas from the previous chapter are repeated here for easy viewing. For example, the "quadratic" formula for SMD for pressure-atomized sprays with swirl or without is given by Eq.(6). We can compare with experimental data([39], [38]) in the two figures below.

A plot of Eq.(6) was shown as solid lines to compare with experimental data for sprays without swirl (Fig.3) and with swirl (Fig.4), corresponding to D32 vs. drop velocity. Those plots originated in Eq.6 soundly assessed in accord with the extents to conceivable physical analysis;

1. If the spray or droplet velocity has not lost (converted) any of its kinetic energy to surface tension energy, i.e. $\overline{u} = u_{inj}$, then the expected drop size is infinity. Physically, this means that no droplets exist, and that the liquid column is intact. As more of the initial kinetic energy is lost through fluid dynamic drag between the liquid and the gas, then the corresponding loss of kinetic energy must appear as surface energy, minus the viscous dissipation. Thus, when $\overline{u} \leq u_{inj}$, the resulting drop size is smaller.
2. Below a certain range, $\overline{u}/u_{inj} \approx 0.75$ for the pressure-atomized sprays without swirl in Fig.3, the decrease in the drop size is gradual with respect to the

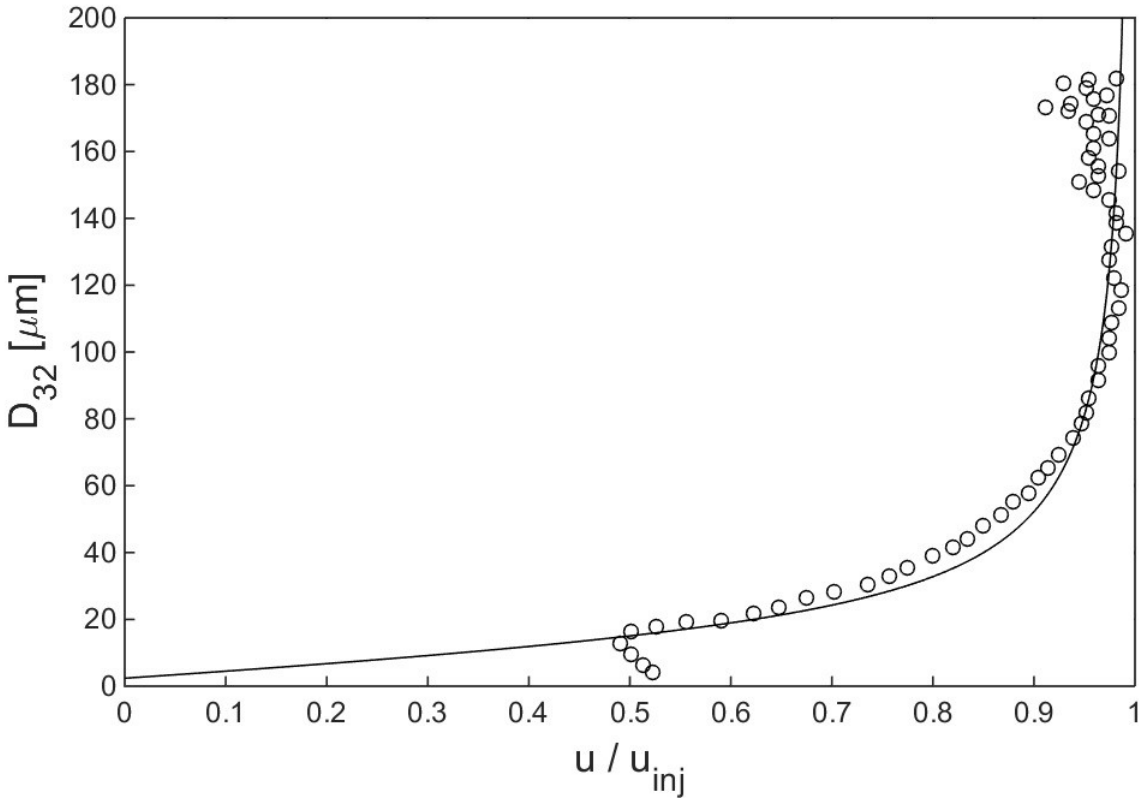

Figure 3. Comparison of the calculated SMD with experimental data of Ruff and Faeth

Experimental data: Ruff and Faeth [39]

velocity decrease, meaning that a near "equilibrium" has been reached for the energy distribution in the spray. A later plot (Fig.5) will show that other parameters such as surface tension and viscosity result in expected trends for the drop size. Thus, the plots in these figures show that there is a "break-up" regime where the velocity of the liquid phase is not substantially different from the injection velocity and the drop size is very large or physically improbable, again meaning that they have not been converted to small droplets. The "atomization" regime is attained when the liquid-phase velocity has been retarded to a sufficient degree, and then the drop size change is relatively small

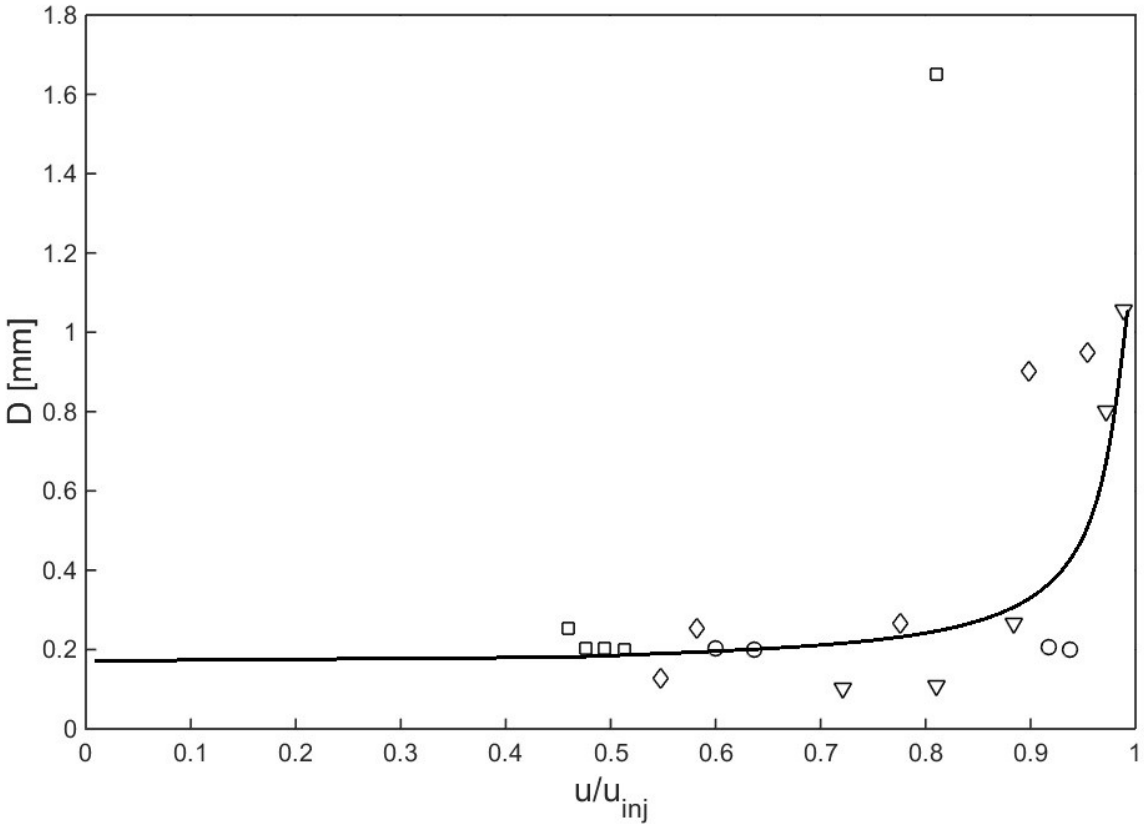

Figure 4. Comparison of the calculated SMD with experimental data of Rimbert and Castanet

Experimental data: Rimbert and Castanet [38]

for any further reductions in the drop velocity. The phenomenon implies this method might substantially useful for estimating the initial drop size in spray computation simulations. In other words, it had good utility toward specifying initial SMD and drop size distributions in computational fluid dynamics of spray flows, either at plane close to the injector or more spatially at the spray boundary. As this method was based on the conservation of mass, energy, and optionally momentum, it characterized free of any non-physical assumptions. The only term to be modeled was the viscous dissipation (the Reynolds number effect); however, it was found a mathematically [40] and physically (Fig.1)

reasonable form. There were quasi-DNS results on spray atomization [17] with which the only adjustable constant, K, in the formulation could be evaluated. The "equilibrium" in liquid energy states should be reached since the energy terms to obtain Eq.(6) was prescribed based on the final drop kinetic and surface energy, along with the viscous dissipation that the liquid phase incurred during the atomization process.

3. A correlation by Wu et al.[50] shows similar asymptotic behavior with current results in Fig.3 and 4. The correlation gives $\mathrm{SMD}/d = 46.4/We^{0.74}$ ([50],[52]), where the Weber number, *We*, is based on the jet speed. Thus, this correlation gives infinite SMD at zero jet speed with rapid decrease toward an asymptotic SMD at high jet speeds. We may reason that this is the same effect observed in our energy balance, where the jet speed is representative of the kinetic energy and zero Weber number corresponds to no kinetic energy available to be converted to surface energy, therefore infinite drop size as in Fig.3 and 4.

There are correlations based on experimental data for SMD. We can also compare Eq.(6) with these correlations, as shown in Fig.5 and Fig.6. The first correlation by Lefebvre [29] for swirl sprays contains the dependence on injection pressure (converted to the injection velocity), viscosity and surface tension. The comparison is reasonable, where the mean spray velocity needs to be estimated in Eq.(6). Once a reasonable estimate is made, the values for both spray velocity and the constant, K', are fixed. Increasing the viscosity results in larger drop size, and the decrease in the surface tension smaller drop size, where the decrease due to the latter effect is somewhat overestimated by Eq.(6). Another correlation by Chen et al. [7] includes the effect of the viscosity, but not surface tension. Eq.(6) generates again favorable comparison,

where the surface tension effect is still present but relatively small for the injection velocities of interest.

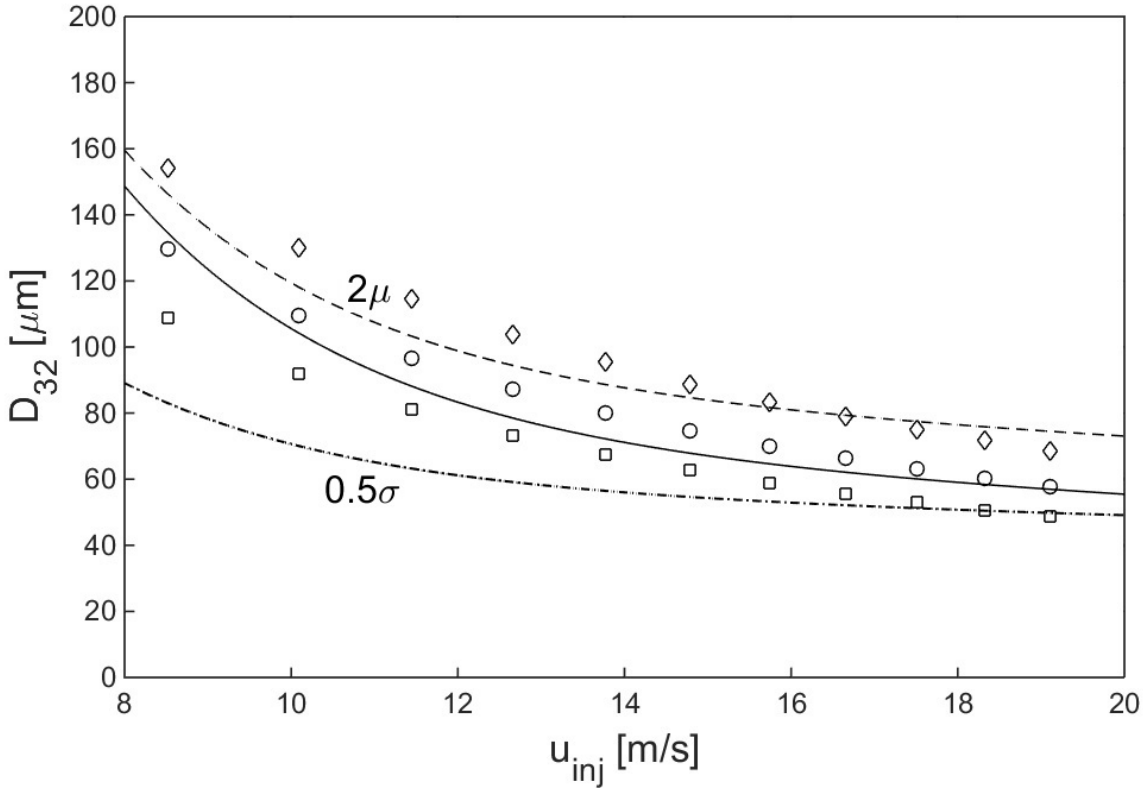

Figure 5. Comparison of SMD with the correlations of Lefebvre
Experimental data: Lefebvre[29]

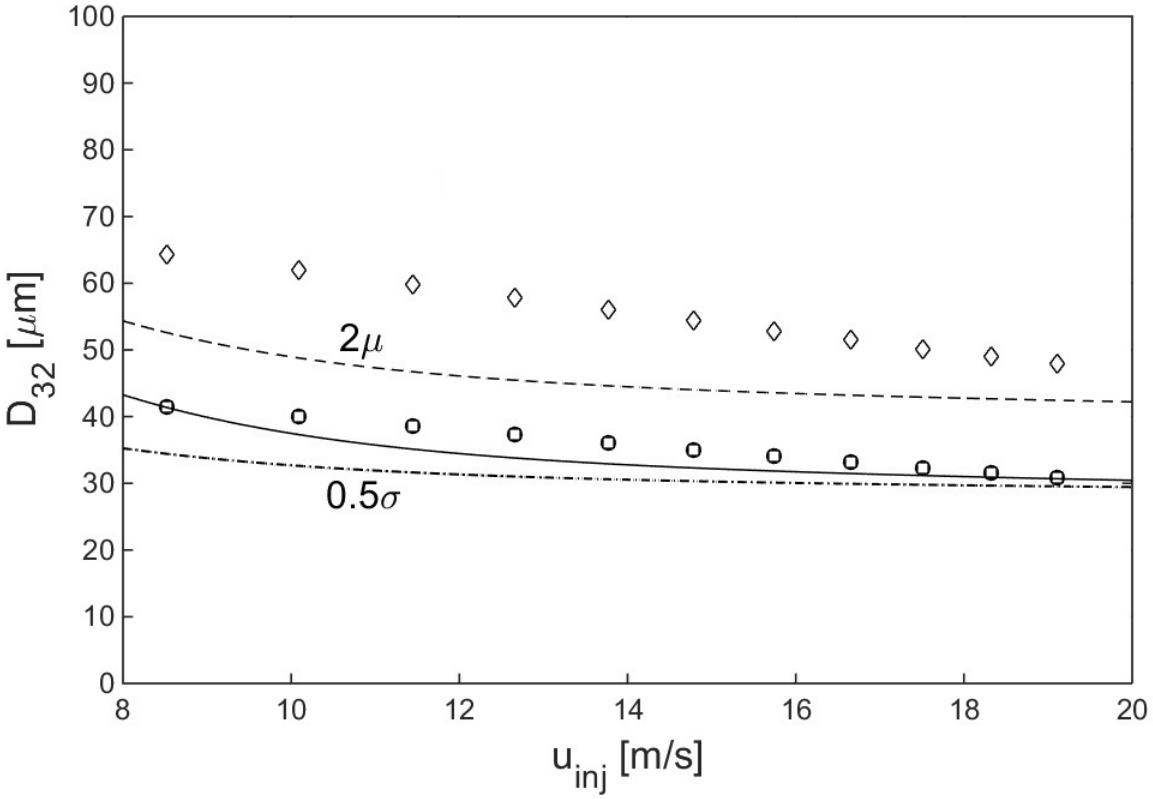

Figure 6. Comparison with SMD with correlations of Chen et al

Experimental data: Chen et al[7]

Recently, we developed a spray drop size calculation module for a CFD company in Tokyo, Japan, called NuFD (Numerical Flow Design). For this work, we further validated the module by using a SMD correlation by Elkotb [10], for straight sprays without swirl. Elkotb's correlation has the following form:

$$D_{32} = 3.08 v_L^{0.385} (\sigma \rho_L)^{0.737} \rho_A^{0.06} \Delta P_L^{-0.54}$$

$$D_{32} = \text{Sauter Mean Diameter}(microns)$$

$$\nu_L = \text{Kinematic viscosity}(m^2/s)$$

$$\sigma = \text{Surface tension}(N/m)$$

$$\rho_L = \text{Density of water}(kg/m^3)$$

$$\rho_A = \text{Density of air}(kg/m^3)$$

$$\Delta P_L = \text{Liquid pressure differential}(bar)$$

From previous work, the following equation(Eq.(6)) can be used for pressure-atomized straight sprays.

$$D_{32} = \frac{3\sigma + \sqrt{9\sigma^2 + K' \rho_L \mu \overline{u}^2 \dfrac{u_{inj}^2 - \overline{u}^2}{2}}}{\rho_L \dfrac{u_{inj}^2 - \overline{u}^2}{2}}$$

A comparison is shown in Fig.7. The liquid (droplet) velocity relative to the injection velocity may vary depending on the location in the spray. For several constant K, it shows quite good agreements with the experimental correlations.

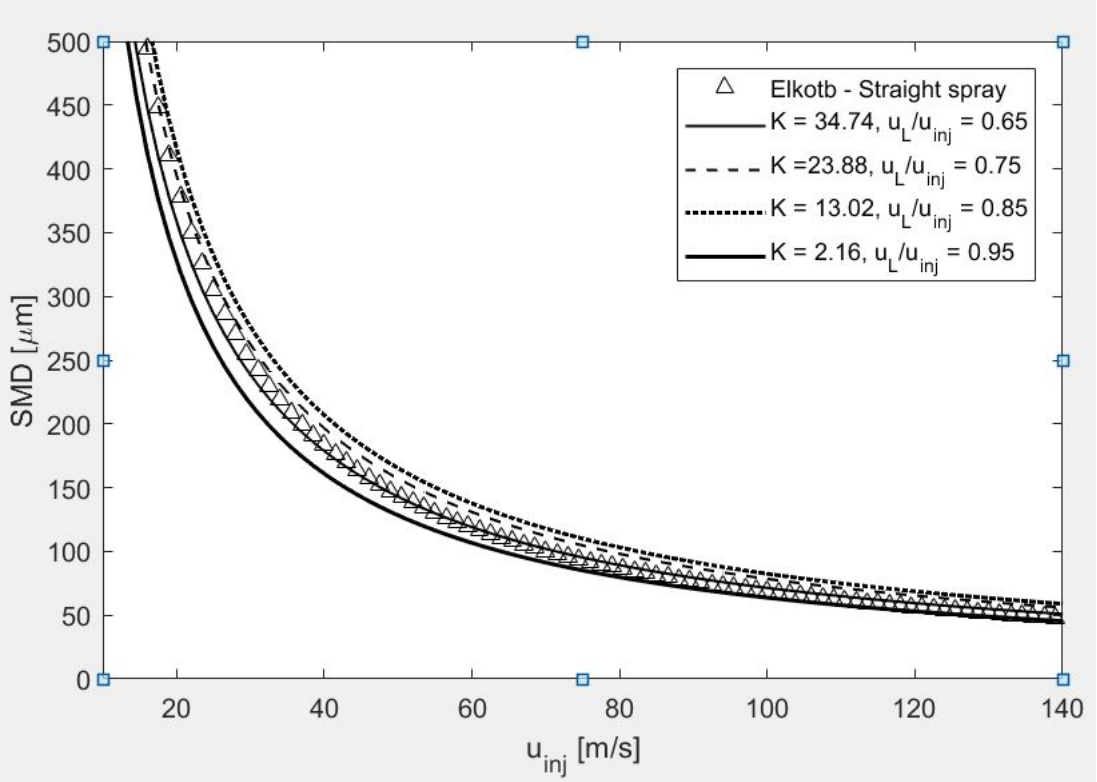

Figure 7. A comparison of the current method with correlation of Elkotb's, for pressure-atomized straight sprays

Experimental data: Elkotb's [10]

We further tested the module for swirl sprays, again using the experimental correlation is by Lefebvre [29].

$$
\begin{aligned}
D_{32} &= 2.2\sigma^{0.25}\mu_L^{0.25}\dot{m}_L^{0.25}\Delta P_L^{-0.5}\rho_A^{-0.25}(microns) \\
D_{32} &= \text{Sauter Mean Diameter}(microns) \\
\sigma &= \text{Surface tension}(N/m) \\
\mu_L &= \text{Viscosity of liquid}(kg/m^3) \\
\dot{m}_L &= \text{Mass flow rate}(kg/s) \\
\Delta P_L &= \text{Liquid pressure differential}(bar) \\
\rho_L &= \text{Density of water}(kg/m^3) \\
\rho_A &= \text{Density of air}(kg/m^3)
\end{aligned}
$$

The drop size equation is the same as Eq.(6), as long as u_{inj} is computed as the square root of the total kinetic energy, as follows:

$$u_{inj} = (u_x^2 + u_\theta^2)^{1/2}$$

For the constant K, the following returns quite good agreements with the experimental correlations. A comparison is shown in Fig.8, where other model results are also included for comparison.

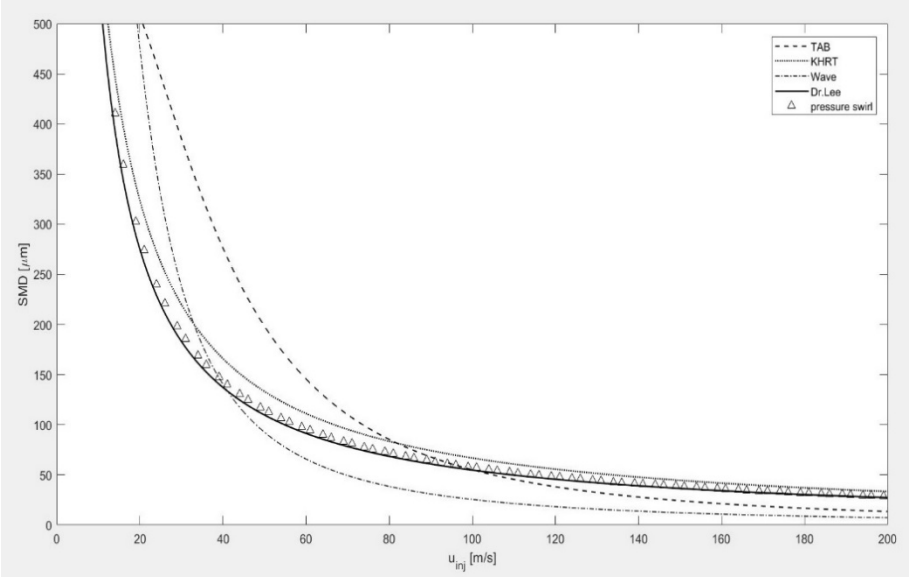

Figure 8. A comparison of the current method with correlation of Lefebvre's, for pressure-atomized swirl sprays

Comparison of all models when $u_L/u_{inj} = 0.4, C = 0.8, K = 6$ in Dr. Lee model, $c_f = 1.5; c_k = 7; c_d = 0.8; c_b = 0.8; y = 1$ in TAB model. B0 =0.15 in Wave model, cdr=1; crt=0.3 in KH-RT model

The experimental data is from Tratnig [47] and includes a large variation in the injector type, swirl, and other injection parameters. This is a good experimental data set to test the current theory, since it varies all the relevant injection parameters, such as the mass flow rate, spray cone angle, and fluid properties. Fig.9 is a comparison of the D_{32}, K and mass flow rate with experimental data. The comparison is not perfect, but given the large variations in the injection conditions, Eq.(6) is useful.

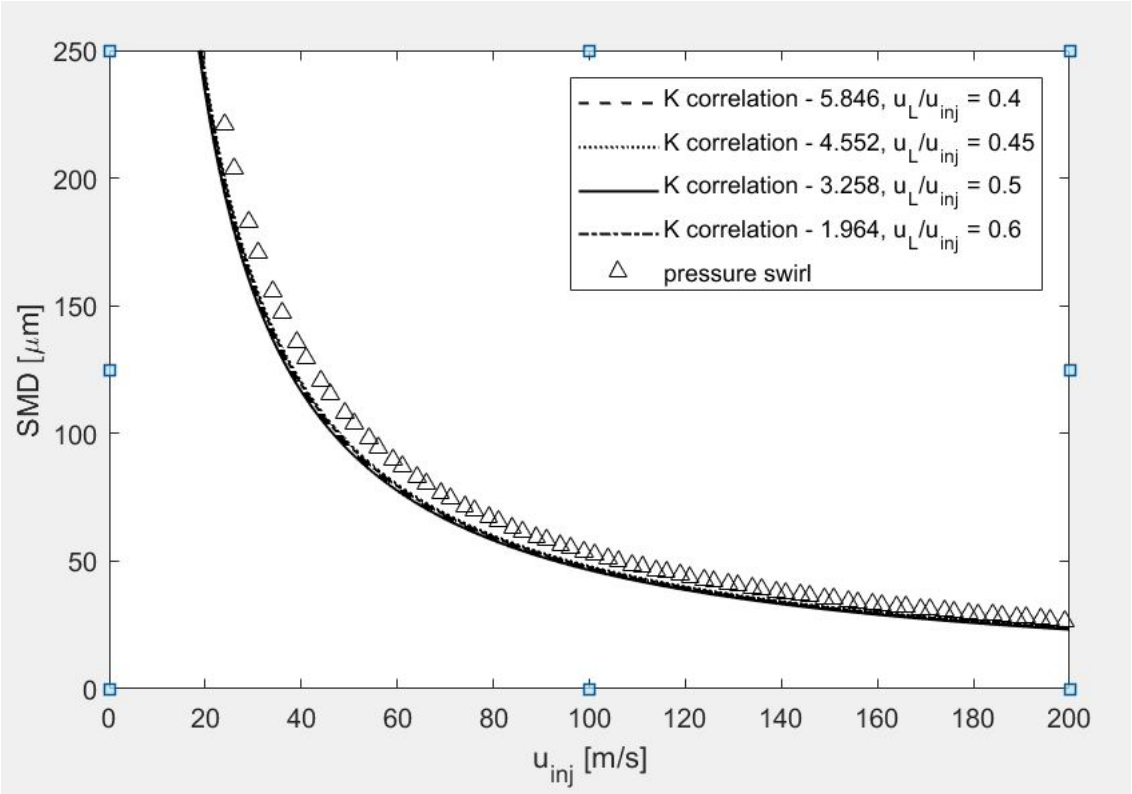

Figure 9. A comparison of the current method with correlation of Tratnig's, for pressure-atomized swirl sprays

Conditions; $\mu_L : 16.26e^{-}3, \sigma : 0.07200, \rho_L : 1240, \rho_A : 1.225, d_{inj} : 0.00076200m$, Experimental data: Tratnig's [47]

The results above are from previous works in this laboratory, and prove that the current approach is viable for sprays with and without swirl. Now the results are presented for the drop size for liquid sprays in cross flows. Fig.10 shows the effect of the incoming gas velocity, u_{in}, on the final drop size using Eq.(14), compared with experimental data of Freitag and Hassa [15] where for low liquid injection velocities (1.3-5.1 m/s) the gas velocity was varied from 50 to 150 m/s. In Fig.10, we can see that there needs to be substantial gas-phase kinetic energy to generate drop size of 100 µm or less. Below u_{in} of approximately 40 m/s, the drop size steeply rises. Dynamically, this has been attributed to the Weber number effect [12, 22, 49], where for the Weber number approaching zero, the drop size tends to infinity [1]. Eq.(14) embodies the underlying energy transfer where the kinetic energy ratio of the incoming and outgoing gas is a determinant for the drop size. Eq.(14) simply shows that this dynamical process can be quantitatively assessed based on relative energy between the incoming kinetic and the rest of the energy terms, in particular surface tension energy. Beyond a certain kinetic energy level ($u_{in} \sim 100m/s$), further decrease in the drop size is gradual and there are diminished returns on increasing the gas-phase velocity. The experimental data show a more gradual decrease of the drop size as a function of the gas velocity than Eq.(14), which may be due to the fact the drop size is a spatial average in the experimental data from Hassa[15]. A velocity distribution would exist after the gas-liquid momentum exchange, leading also to a range of drop size for a given inlet condition. The experimental data of Freitag and Hassa [15] shows a variation in the SMD (up to 43%) within the measurement plane. Thus, SMD is not uniform, as the velocity field is not uniform. Eq.(11) indeed shows this would be the case if there is a velocity variation. The theoretical results (lines) used in Fig.10 are effectively the specific value of SMD at a given velocity. Since the relationship between

the SMD and the velocity is non-linear as shown in Eq.(14), spatial averaging can lead to some discrepancy. More explanation will be said later about this relationship between the drop size and final gas velocity (u_{out}) distribution. The experimental data show a weak dependence on the injector diameter, where the drop size increases with the injector diameter [15].

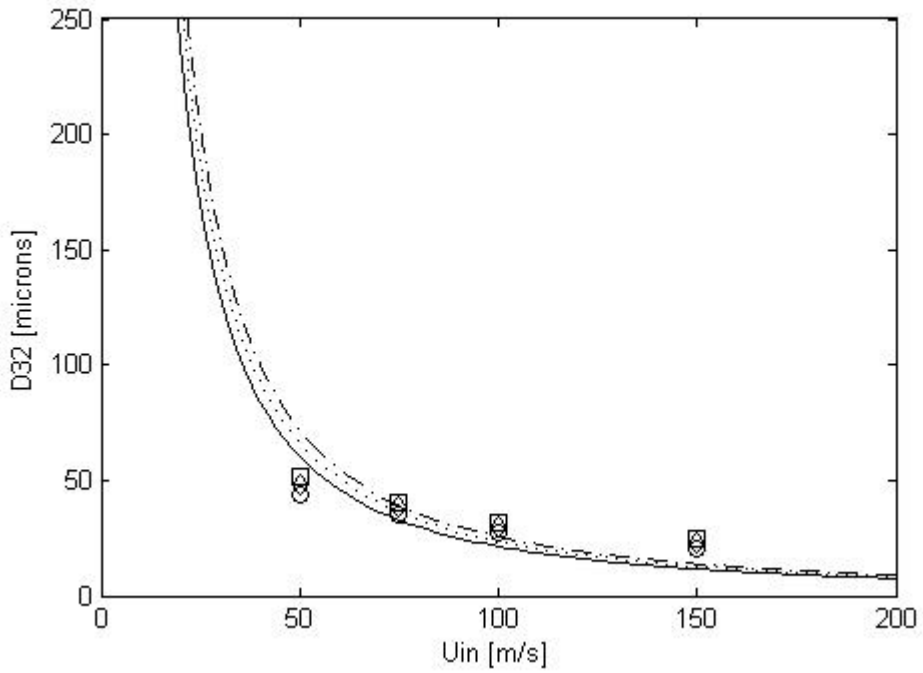

Figure 10. Effect of incoming gas velocity on the SMD

Three different injector diameters: 0.3 mm (∘, solid line), 0.5 (⋄, dotted line), 0.7 (□, dashed line). The experimental data from Freitag and Hassa[15] are plotted as symbols.

Fig.11 is a similar comparison showing the effects of gas density or the gas pressure. In Freitag and Hassa[15], the air pressure was varied from 0.2 to 0.8 MPa. The pressure effect appears as the gas density effect in Eq.(14), as the gas density will increase proportionally with the pressure. Since the gas-phase kinetic energy flow

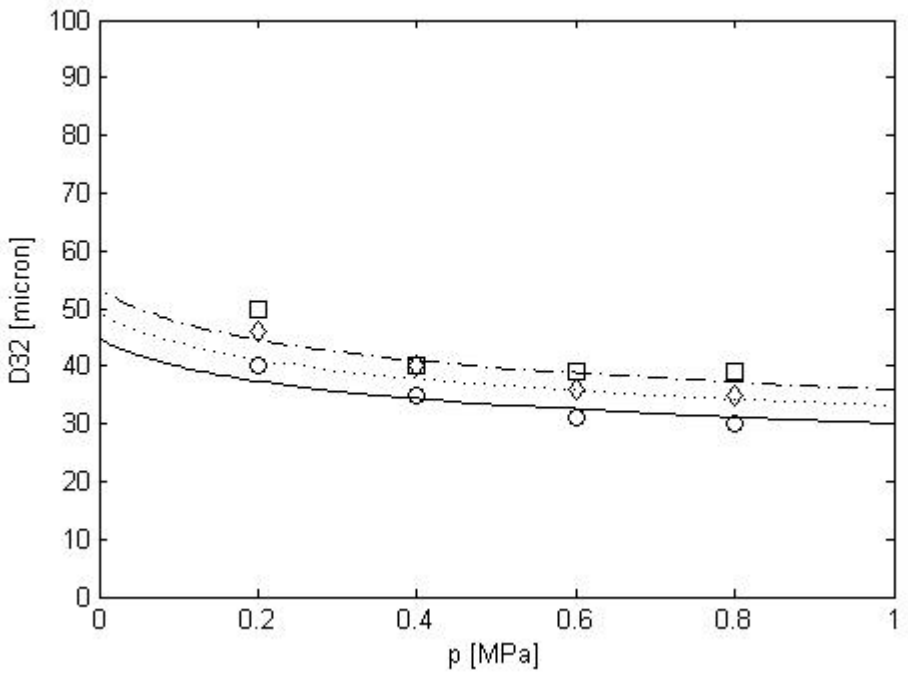

Figure 11. Effect of gas pressure (density) on the SMD

Three different injector diameters: 0.3 mm (∘, solid line), 0.5 (⋄, dotted line), 0.7 (□, dashed line). The experimental data from Freitag and Hassa[15] are plotted as symbols.

rate is linear with the density (as opposed to cubic dependence on the velocity), the decrease in the drop size with increasing density is relatively small in Fig.11. This is due to the cubic term for u_{out}/u_{in} in Eq.(14). For large u_{in}, the kinetic energy contribution to the drop formation rapidly approaches its maximum.

Other authors present the data in different ways, and drop size dependence on relevant injection parameters can still be retrieved from some of those data sets. For example, Shafaee et al.[42] also present the SMD measured at a fixed location, as a function of the gas velocity for various injector diameters. These results are plotted in Fig.12, where injector diameters were 0.8, 1.2, 1.6 and 1.8 mm. Although the injector diameters were varied, the mass flow rate was fixed. Thus, the injector diameter

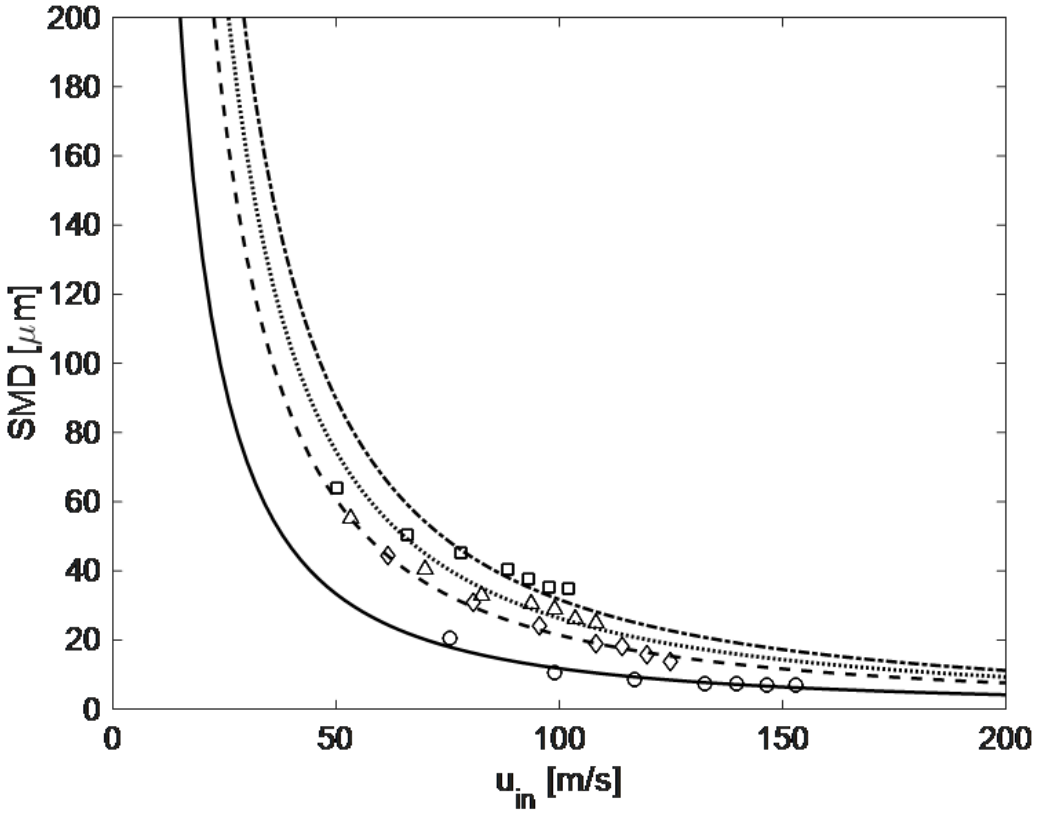

Figure 12. Comparison of the measured and calculated SMD

Four injector diameters were used: d_{inj} = 0.8 mm (○, solid line), 1.2 (◇, dashed), 1.6 (△, dotted), 1.8 (□, dash-dot). The experimental data from Shafaee et al.[42].

essentially varied the momentum ratio and also the spray volume. The parameter, K', in Eq.(14) for the viscous dissipation term contains the spray volume term. Any changes in the spray volume should be taken into account where the spray volume would increase with the injector diameter. K' increases with the injector diameter (spray volume), and they are adjusted to provide an agreement at a given u_{in}. K' is then held fixed for each injector diameter. K' were set at 0.9, 6.7, 18 and 33, respectively, for injector diameters of 0.8, 1.2, 1.6 and 1.8 mm. A systematic method to estimate K' in various spray geometry is currently being investigated.

The drop size change, as a function of the gas velocity for various injector diameters (momentum ratios), is again quite well tracked by Eq.(14), as shown in Fig.12. Also Fig.12 shows that the change in SMD is gradual relative to the gas velocity beyond a certain gas velocity range (about $u_{in} = 100m/s$ in Fig.12). Similar observations have been made where SMD change was relatively small in comparison to large increases in the gas velocities. The agreement between the data and theory is quite good for $d_{inj} = 0.8$ and 1.2 mm in Fig.12. For larger injector diameters (1.6 and 1.8 mm), the change in SMD with increasing u_{in} is small in comparison to the current results. For larger injector diameters, the spray volume is larger, and therefore the potential for spatial averaging bias (mentioned earlier) is larger. Larger drop sizes also mean possible presence of non-spherical or even ligaments, which will not appear in drop size measurements based on sphericity of droplets, thus biasing down the measured SMD. Nonetheless, the trend toward increase in drop size relative to u_{in} and d_{inj} are well reproduced by the theoretical lines.

Kihm et al.[21] presents a drop size correlation in terms of Reynolds and Weber numbers along the spray arc length (x and y in their notations). We usually prefer to apply Eq.(14) to a fixed position far downstream, as the drop size data typically exhibit decreasing trend with increasing distance from the injectors. However, the asymptotic location (the location where the drop size no longer changes) is not easily reached, either dynamically or experimentally. Also, in an attempt to account for all of the relevant parameters, such as gas velocity, injection velocity, densities, surface tension and viscosities, the range of gas velocity that was varied in the experiments [21] was not significant enough to produce a large change in the drop size, as shown in Fig.13. The y/d_{inj} locations varied from 35, 40 to 45 in Kihm et al.[21]. In spite of the fact that the measurement locations are varied, we can argue that the u_{out}/u_{in} to be

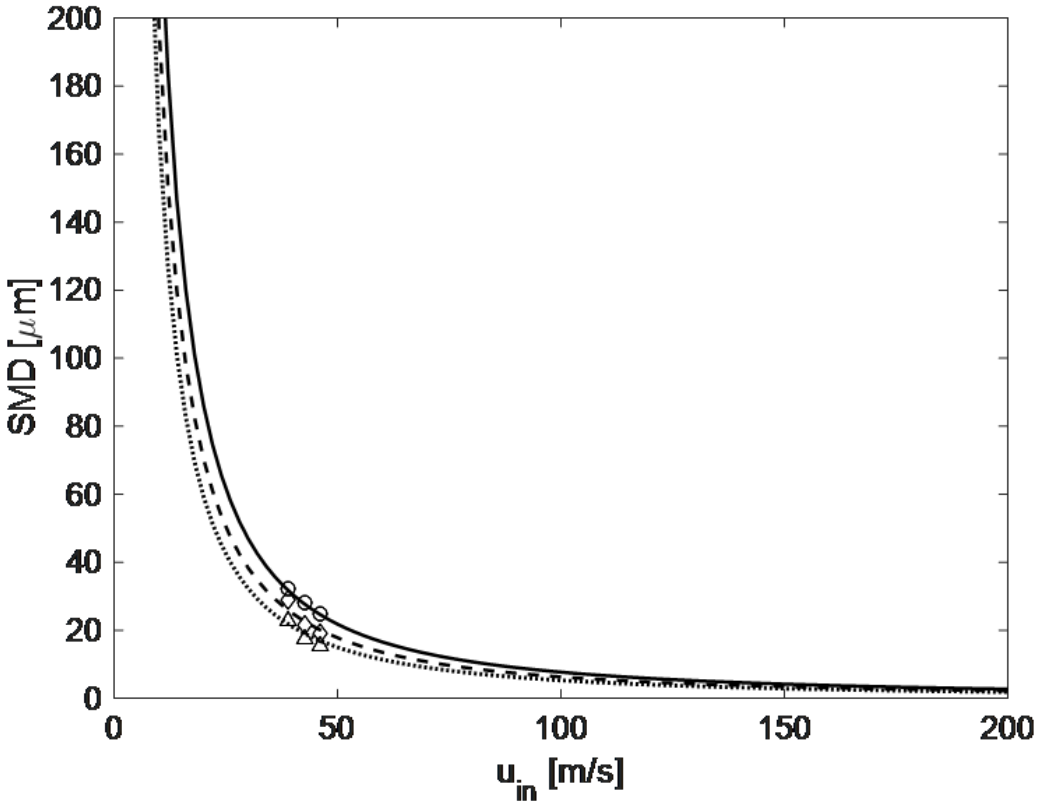

Figure 13. Comparison of the measured and calculated SMD at various locations $y/d_{inj} = 35$, solid line ($\circ$); $y/d_{inj} = 40$, dashed ($\diamond$), $y/d_{inj} = 45$, dotted ($\triangle$). The experimental data from kihm et al.[21].

input into Eq.(14) should decrease as the liquid and gas phases exchange momentum further along the liquid trajectory, resulting in liquid phase gaining momentum and the gas phase losing momentum. Fig.13 shows a comparison of the drop size with that calculated using Eq.(14), where u_{out} of 0.57, 0.75, and 0.85 u_{in} were used for y/d_{inj} locations of 35, 40 and 45, respectively. K was fixed at 2.55. Although this required some optimization of the unknown u_{out}/u_{in} ratio, the trend in the drop size as a function of gas velocity is captured quite closely at various locations in the spray. As in our previous work[26], momentum equations for the gas and liquid phase can

be used to estimate u_{out}/u_{in}, or computational simulations can be augmented with Eq.(14) to iteratively determine the drop size and u_{out}/u_{in}.

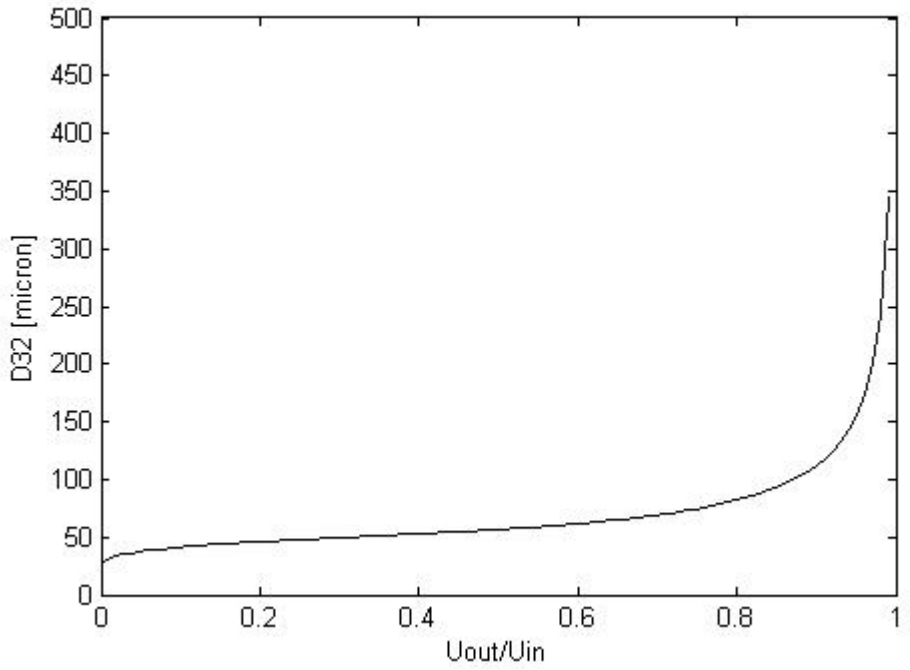

Figure 14. Effect of the gas-phase velocity ratio on the SMD

Fig.14 is a representation of the effect of u_{out}/u_{in} on the drop size, and also can be used as a direct relationship between the velocities and drop size. Eq.(11) points to a cubic increase in the drop size with u_{out}/u_{in}. When $u_{out} \rightarrow u_{in}$, no gas-phase kinetic energy has gone into the atomization process, and the drop size is infinite. Dynamically, the aerodynamic interaction between the liquid and gas phase will result in momentum exchange through the drag force, with the gas-phase momentum going into liquid momentum in the stream wise (for the gas-flow) direction. This will also be represented as kinetic energy loss for the gas phase, along with the requisite surface tension energy when droplet curvatures are generated according to Eq.(14). Thus, the larger the energy loss, or equivalently the lower the outgoing gas velocity relative to a

fixed u_{in}, smaller drop size will result. It is interesting to note that below u_{out}/u_{in} 0.8, the drop size change is relatively gradual, with drastic changes occurring for u_{out}/u_{in} from about 0.85 to 1, due to the cubic shape of the curve. A similar behavior has been observed for secondary atomization where the kinetic energy difference between the incoming and exiting gas causes the parent droplet to break up into a group of small droplets [27].

Above results and Eq.(14) show that crossflow atomization under typical injection conditions is primarily determined by the ratio of the incoming to outgoing gas velocity. The reason is evident from the energy balance: if more of the kinetic energy of the gas that goes into the surface tension energy, then smaller droplets will be formed. In other words, the larger the difference (or the ratio) between the outgoing and incoming gas velocities, the drop size will become smaller. We saw this effect of incoming gas velocity in Fig.10. Fig.14 also hints at a self-consistent method for embedding the cubic formula (Eq.(14)) in computations of sprays in cross flows. For example, data on gas velocity distribution at the exit plane can be converted to the drop size distribution through Eq.(14). This process is illustrated in Fig.15 and 16.

In Fig.15 and 16 shows where starting from some gas velocity distribution (Gaussian or reversed log-normal in Fig.15) so we can generate the drop size distributions using Eq.(14) as shown in Fig.16. Eq.(14) can therefore be used as the drop size-velocity cross-correlator. In Fig.16, the reversed log-normal distribution leads to a drop size distribution with a wide spread, while the Gaussian results in a distribution sharply peaked at a small drop diameter.

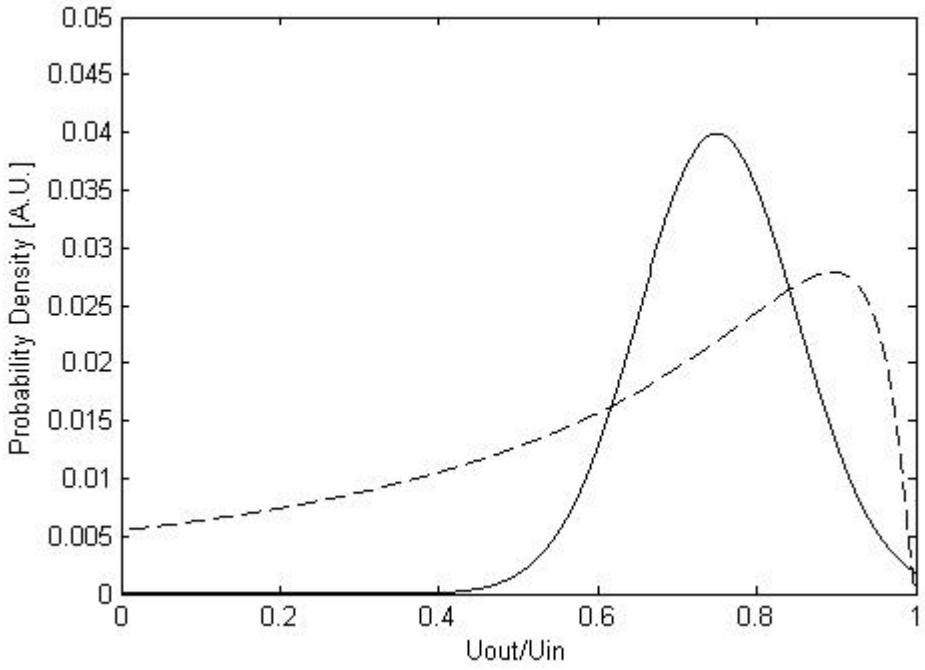

Figure 15. Examples of probability density function for the velocity ratio, u_{out}/u_{in} ——— (Gausian); - - - - (reversed log-normal)

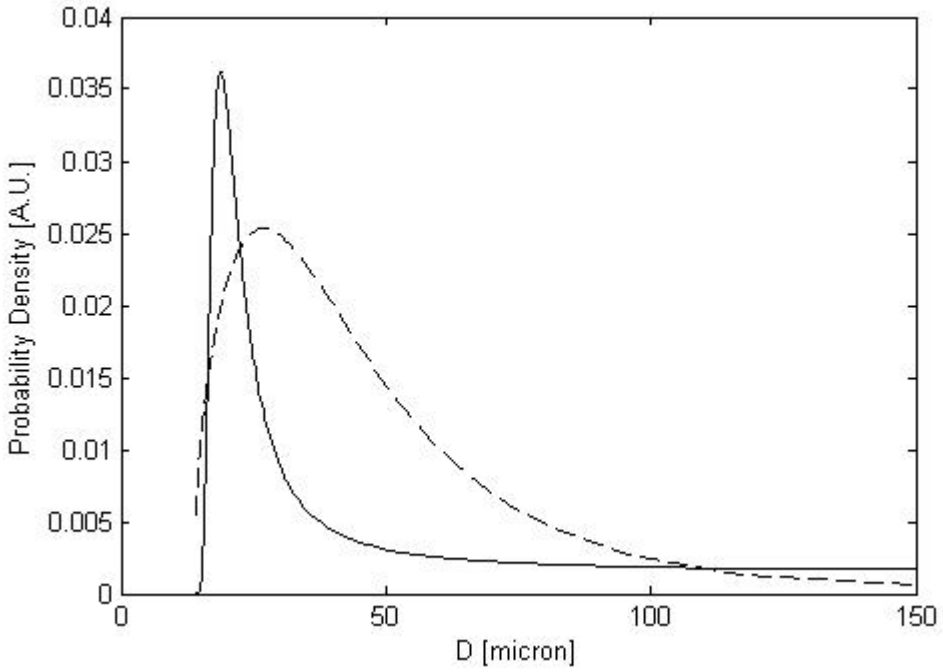

Figure 16. Resulting drop size distribution using Eq. 14

——— (from Gausian); - - - - (from reversed log-normal)

We can compare with the drop size distribution as reported by Song et al.[44] at two Weber numbers of 500 and 1000, as shown below.

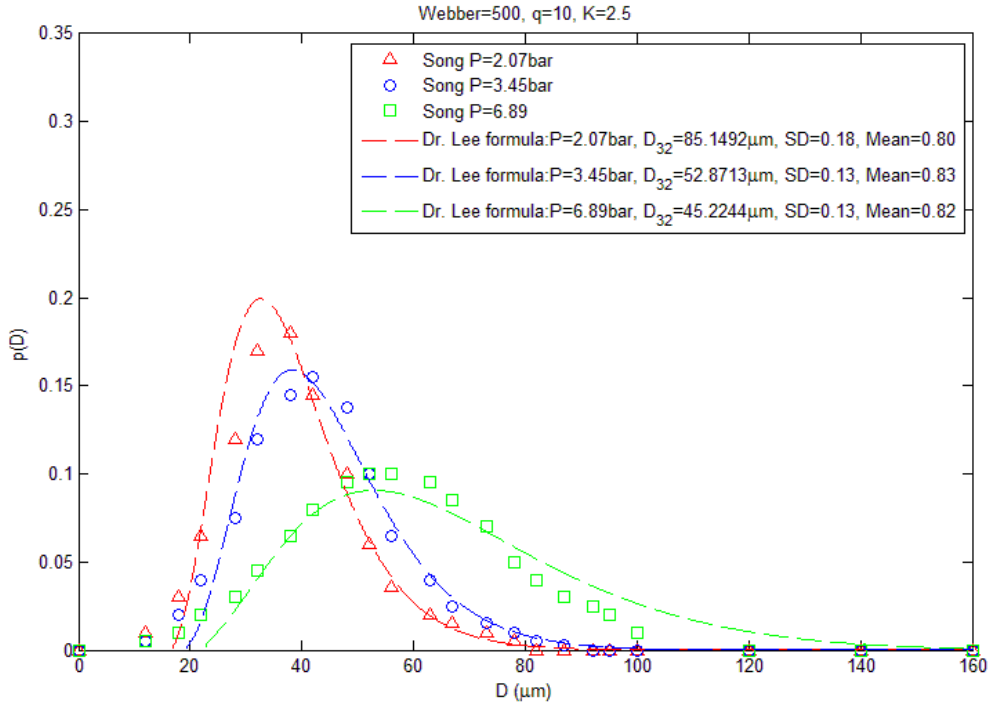

Figure 17. Comparison of the drop size distribution with experimental data, We=500 Experimental data: song et al.[44]

Song et al.[44] also came up with a correlation based on their experimental data. We can compare with the D32 results with that correlation. Solid blue line is Eq.(14), and the red dots represent the correlation by Song et al.[44]. We can see that even though the correlation gives larger drop size at identical conditions, both results point to atomization being inefficient below about 50 m/s. Also, the decrease in drop size with increasing air velocity becomes gradual beyond 140 m/s. This means that there

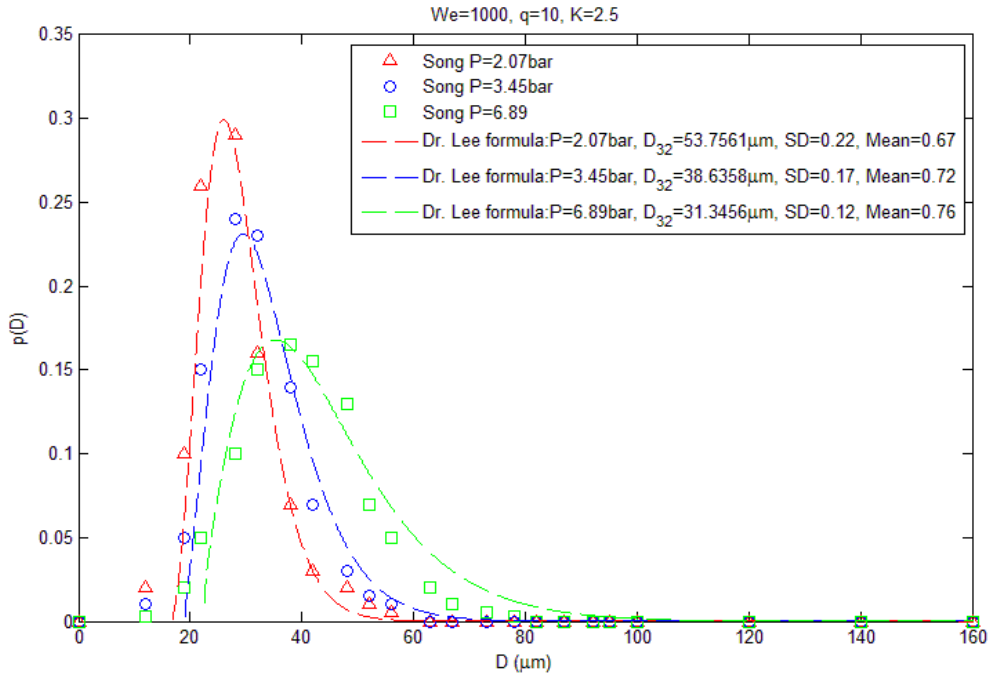

Figure 18. Comparison of the drop size distribution with experimental data, We=1000

Experimental data: song et al.[44]

is a range of optimum air velocities below which the liquid is not properly atomized or beyond which there is diminishing gain for increasing the air speed.

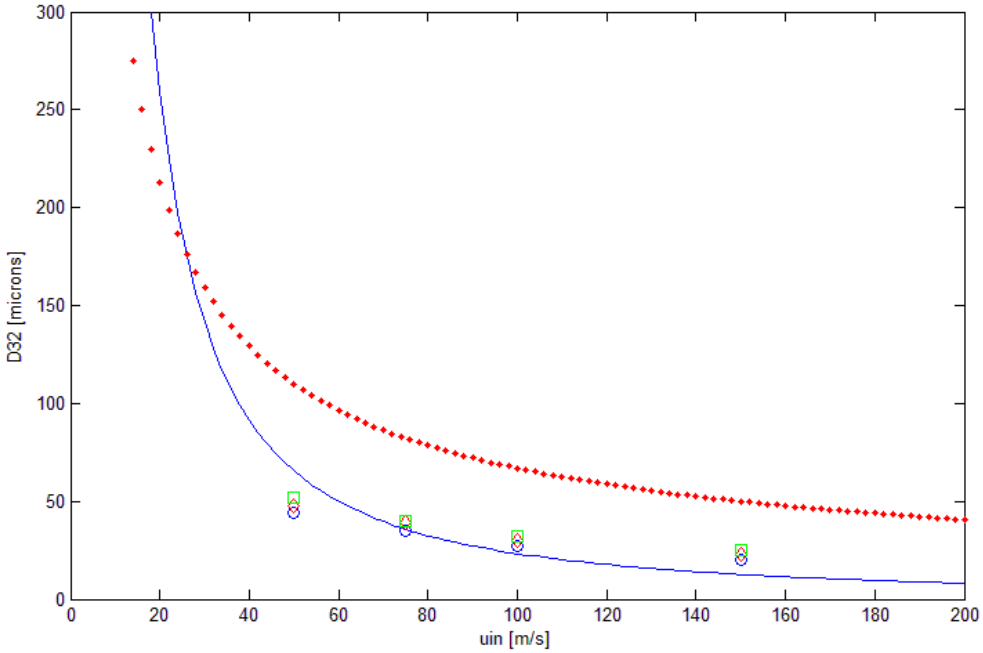

Figure 19. Comparison of the drop size correlation

From song et al.[44]

3.1 A Generalized Formulation for Determination of Drop Size in Sprays

Recently, we realized that a general formulation for determination of drop size is possible for all spray configurations. Fig.20 shows a schematic of flows where there is a gas flow at an arbitrary angle, θ, relative to the liquid spray. If there is no air flow, then we have pressure-atomized sprays with or without swirl. If there is a cross flow, then the angle, θ, is 90°. If $\theta = 0°$, then it would be a co-annular flow geometry. We realize that for cross flow component, it is the sine component that is the driving mechanism for the atomization, e.g. liquid sprays in cross flows as discussed above. On the other hand, the cosine component reduces the aerodynamic shear between the liquid and the surrounding air so that it would have retarding effect on spray atomization. For example, if the liquid and the gas had exactly the same velocity field, then there would be no mechanism for Kelvin-Helmholtz type of instabilities, nor any liquid atomization. For this reason, the sine component of the air velocity needs to be subtracted from the injection velocity. After making these corrections to the velocity components, we can obtain a general formula for determination of the drop size in spray flows. For air-blast atomization, then there will be some angle θ between 0° and 90°, and typically both the liquid and gas velocities activate the atomization mechanisms.

We make the following transforms:

$$u_{inj} \rightarrow u_{inj} - u_{in} \cos\theta$$

$$u_{in} \rightarrow u_{in} \sin\theta$$

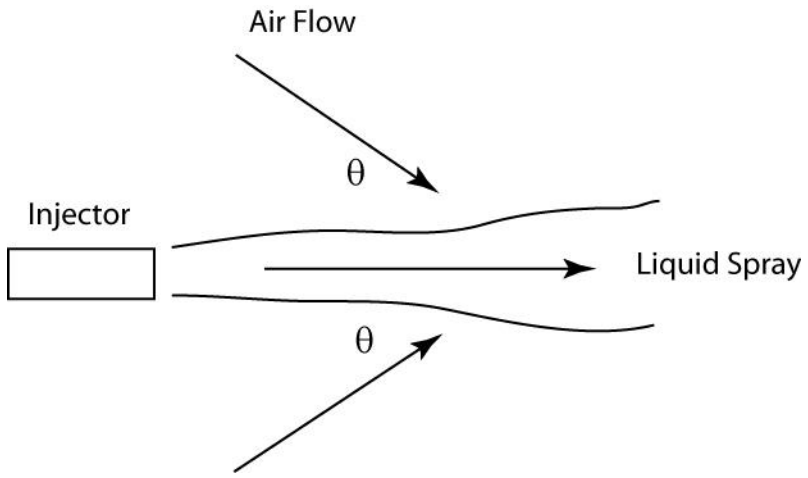

Figure 20. A schematic for the general formulation for determination of drop size in spray flows

The transform to $u_{inj} - u_{in}\cos\theta$ requires either a square or absolute sign, since for some co-flow air-blast atomization $u_{in}\cos\theta$ can exceed u_{inj} to promote atomization. This gives us the following formula for D_{32} in spray flows:

$$D_{32} = \frac{3\sigma + \sqrt{9\sigma^2 + \frac{K\mu_L u_L^2}{\left|u_{inj} - u_{in}\cos\theta\right| A_{inj}}\left[\frac{\rho_L (u_{inj} - u_{in}\cos\theta)^2}{2}\left(1 - \left(\frac{u_L}{(u_{inj} - u_{in}\cos\theta)}\right)^2\right) + \frac{u_{in}\sin\theta A_c}{\left|u_{inj} - u_{in}\cos\theta\right| A_{inj}}\frac{\rho_g (u_{in}\sin\theta)^2}{2}\left(1 - \left(\frac{u_{out}}{u_{in}\sin\theta}\right)^3\right)\right]}}{\left[\frac{\rho_L (u_{inj} - u_{in}\cos\theta)^2}{2}\left(1 - \left(\frac{u_L}{(u_{inj} - u_{in}\cos\theta)}\right)^2\right) + \frac{u_{in}\sin\theta A_c}{\left|u_{inj} - u_{in}\cos\theta\right| A_{inj}}\frac{\rho_g (u_{in}\sin\theta)^2}{2}\left(1 - \left(\frac{u_{out}}{u_{in}\sin\theta}\right)^3\right)\right]} \tag{15}$$

The accuracy of this approach is currently being investigated, by comparing with experimental data for air-blast and air-assisted atomization. We can see in the figure below that the air stream angle, θ, has a large effect on the resulting drop size, according to Eq.(15). For $\theta = 15°$, the drop size is very large above 500 μm. Even at for $\theta = 45°$ and $60°$ the atomization due to impinging air is not very effective. At $\theta = 90°$, the atomization is due to cross flow and we obtain the same result as in above.

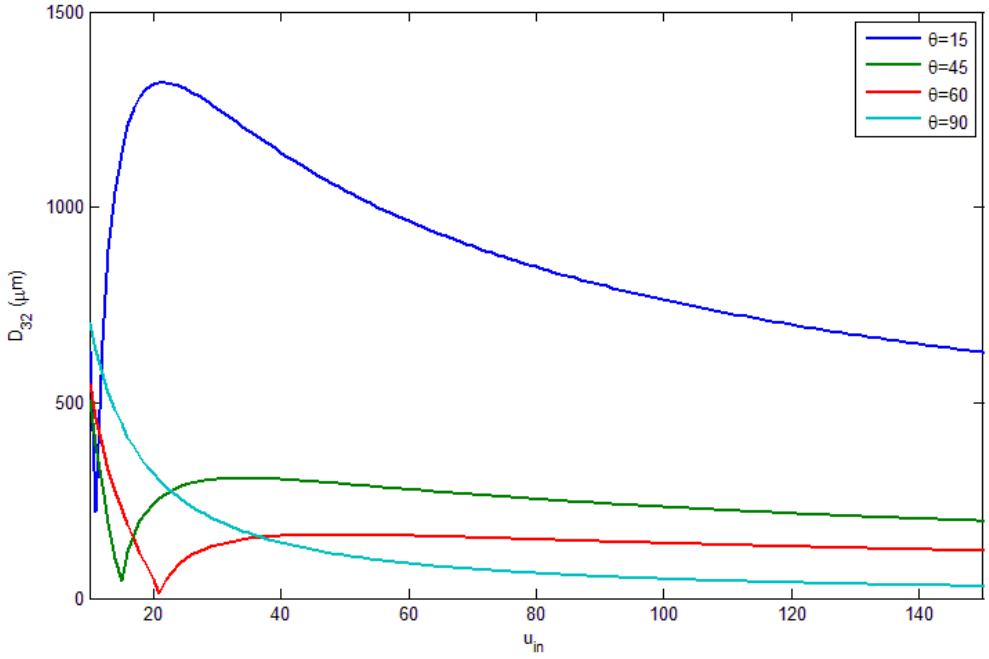

Figure 21. A schematic for the general formulation for determination of drop size in spray flows

However, it can be guessed that this is a more difficult problem than previous cases because the velocity fields will be quite different depending on the angle, θ. This means that the ratio of the injection to the final liquid velocities, and the ratio of the incoming to exiting gas velocities, will differ as the angle changes. For example, at small θ the flow is similar to a boundary layer flow and the gas velocity will be equal to the liquid velocity at the liquid-air interface. On the other hand, at large θ the liquid core acts somewhat like a bluff body so that the final change in liquid and gas kinetic energy, an important factor in the current set of formulas, will all be different as a function of θ. Thus, a fully generalized formulation will require a simultaneous fluid momentum analysis. The validity of this approach needs to be further checked using experimental data.

Chapter 4

CONCLUSIONS: APPLICATIONS TO CFD

First, I review the previous work done in this laboratory for application of the current method for CFD. In computational fluid dynamics (CFD) of sprays, including spray evaporation and combustion, setting the initial conditions for the drop size and velocity has been the biggest hurdle in accurate simulations. Once the initial drop size and velocity are properly set, then there are several reliable methods for subsequent tracking of the particles, such as particle-in-cell (Eulerian-Lagrangian) calculations. Phase change, mass and energy transfers, can also be effectively treated using thermodynamic modules. Thus, a capability to specify the droplet initial conditions, based on the first principles, is of utmost necessity, to replace the *ad-hoc* models presently used in many commercially available software packages. We start by taking note of the fact that the energy balance used in Eq.(6) can be used between any two locations. In Fig.1, we have applied the method from the injector exit to the "atomization plane", where the liquid core has completely disintegrated and atomized into spherical droplets. In compact sprays, such as swirl sprays, this may be an ideal application since the spray initial conditions can be set at a location close to the injector exit. But what about pressure-atomized sprays without swirl, such as Diesel sprays, with atomization lengths typically observed at x/d of 100 to 200. Much can happen within the volume that extends to such large axial locations, in terms of fuel mixing and combustion, for instance. Thus, it is necessary to set the initial conditions in a different manner.

If we again look at results in Fig.3 and Fig.4, we can see that it is possible to use the velocity information to set the initial SMD, since the quadratic formula Eq.(6) provides a direct velocity-drop size relation. Also, from such plots, we can obtain estimates for the maximum and minimum drop size, to determine the general shape, variance term, of the drop size distribution. In this regard, we note that the liquid-phase velocities are quite accurately computed by computational methods. For example, Fig.22 shows the average liquid velocity as a function of x/d for a liquid jet at injection velocity of 56 m/s, the same as the experiment by Ruff and Faeth [39]. Although the centerline velocity persists at a level close to the injection velocity to a large axial location, velocity averaged over the cross-section of the liquid jet undergoes a transition to lower value much earlier, as seen in Fig.22. Thus, we can use this average liquid velocity to find the SMD's as a function of x/d, again using Eq.(6), which are overlaid in Fig.22 for various values of K. We can see that the initial SMD tend to be quite large, 800 to 1400 µm, depending on K, and drops to 250 to 450 μm range, when the average liquid velocity has been retarded by x/d $\sim$ 15. Thus, we can use the SMD calculated using Eq.(6) at, say, x/d = 5 to set the initial SMD. Subsequent computations of the spray flow to track drop motion and dispersions (that can cause variations in the SMD at axial and radial locations) show quite good agreement with Ruff and Faeth [39], as shown in Fig.23. Fig.23 shows the CFD results for SMD along with drop velocity as a function of the radial location, as computed using initial SMD specified at x/d = 5 and $K' = 0.06$. For initial SMD specification, only one value of K' is needed. However, for local SMD calculations, K' increases nearly linearly with x/D since it contains the spray volume term Eq.(3). These are compared with SMD measurements of Ruff and Faeth [39], and again confirmed with Eq.(6) that relates the drop velocity with SMD at the same location. Although the initial SMD was set at a location close

to the injector (x/d = 5) in Fig.23 for comparison with data at x/d = 12.5, 25, 50 and 100, for most simulations SMD initial condition should be set beyond x/d = 15, where the transition to the equilibrium liquid momentum and therefore SMD is achieved as shown in Fig.22.

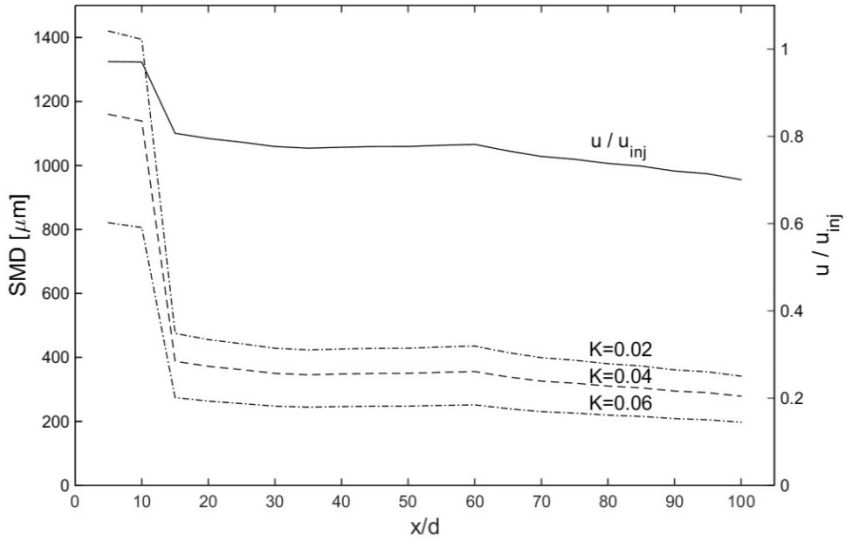

Figure 22. SMD calculated from CFD-generated average liquid velocities
CFD is for a liquid jet, with no droplets in the flow

Fig.23 shows the SMD remains high near the centerline, mainly because x/d locations are well below the so-called atomization length. Lower SMD are observed near the periphery of the spray, as smaller droplets preferentially disperse toward regions of lower velocity. This observation also points to a method for more spatially-detailed specifications of the initial drop size. That is, instead of initiating the spray calculations at a plane (x/d = 5 in the above example) close to the injector exit, we can specify the drop initial conditions at the spray "boundary layer", which corresponds to the regions where atomization is taking place from the liquid surface

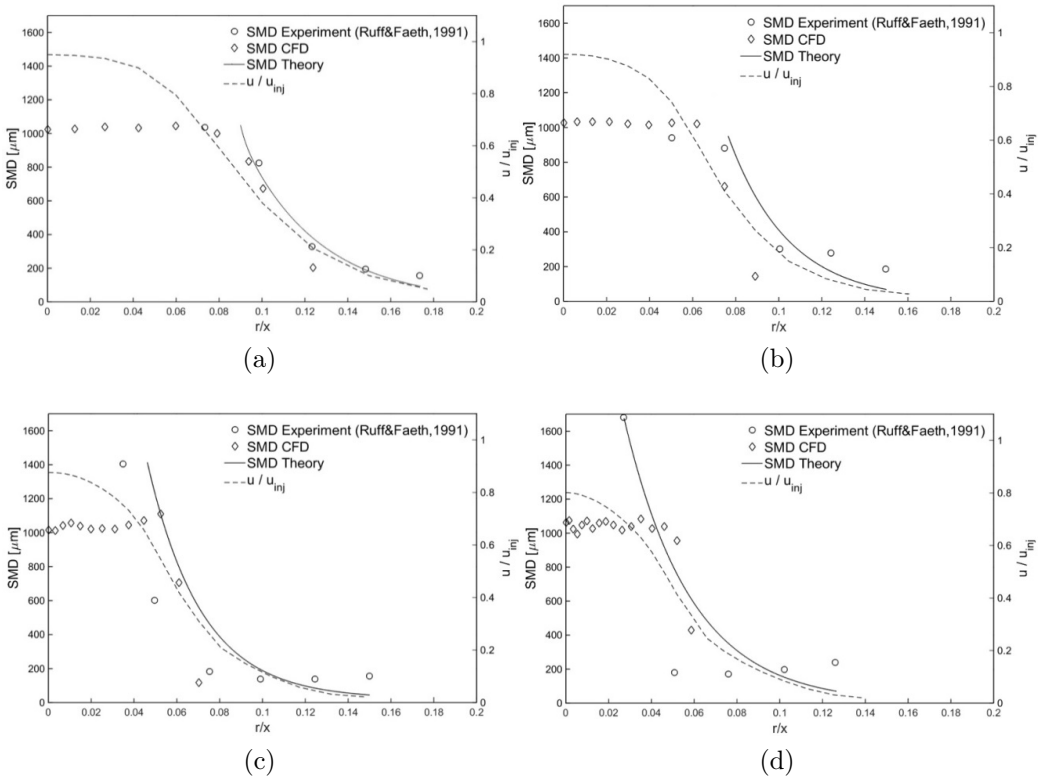

Figure 23. Comparison of the SMD, measured, calculated and also from CFD-generated liquid velocities

CFD is for a spray flow, with droplets released at x/d = 5. The plots are for x/d = 12.5(a), 25(b), 50(c) and 100(d)

in the pressure-atomized sprays. This will amount to a two-dimensional specification of the drop initial conditions, where the SMD and velocities are specified at the inner radial location (close to the liquid-air interface). We take the advantage of the fact that close to the injector, the liquid velocities (shown as dotted lines in Fig.23) tend to be independent of the drop size as the momentum is dominated by the initial inertia of the injection. The available liquid velocity can then be converted to local SMD as in Fig.23.

An alternative method for spatial specification of the initial drop size is to use the CFD results for axi-symmetric, columnar liquid jet (Fig.22 directly, at the same

initial spray injection conditions (injection velocity, injector diameter, and liquid properties), and again use the velocity data from such simulations, as shown in Fig.24. We immediately see that the liquid velocity profiles are much more compact than the actual spray flow, since the liquid column does not spread out as much as the droplet-laden flow in Fig.23. However, the SMD values are again close to the experimental data [39], albeit at smaller radial locations. Thus, we can "release" the droplets of the calculated SMD's at the inner spray at the CFD-generated liquid velocity vectors (axial and radial components) to provide the local initial droplet conditions in spray simulations.

As noted earlier, for a fixed drop size, D_{32} in Eq.(6) simply reduces to D as a function of drop velocity, providing essentially the cross-correlation between the drop size and velocity. This can be used to construct the drop size distribution, in addition to the SMD. There are on-going works by other researchers [33, 50, 52] to determine the exact drop velocity distributions which may deviate from conventional clipped-Gaussian probability density function. For the purpose of demonstrating the transform from the drop velocity to drop size distributions, we take the simple clipped-Gaussian and use Eq.(6) to determine the drop size distribution, as shown in Fig.25. Due to the asymptotic behavior for drop size as a function a liquid velocity, there is a shift toward smaller drop size and a long tail in the large drop size, which is the drop size distribution observed in sprays. For the velocity distribution centered at larger liquid speeds, the corresponding drop size distribution is shifted toward much larger drop size due to the steep slope of u-D relationship near u_{inj}. When more exact velocity distributions are known from CFD or other means, then it can be easily converted to the drop size distribution using this approach.

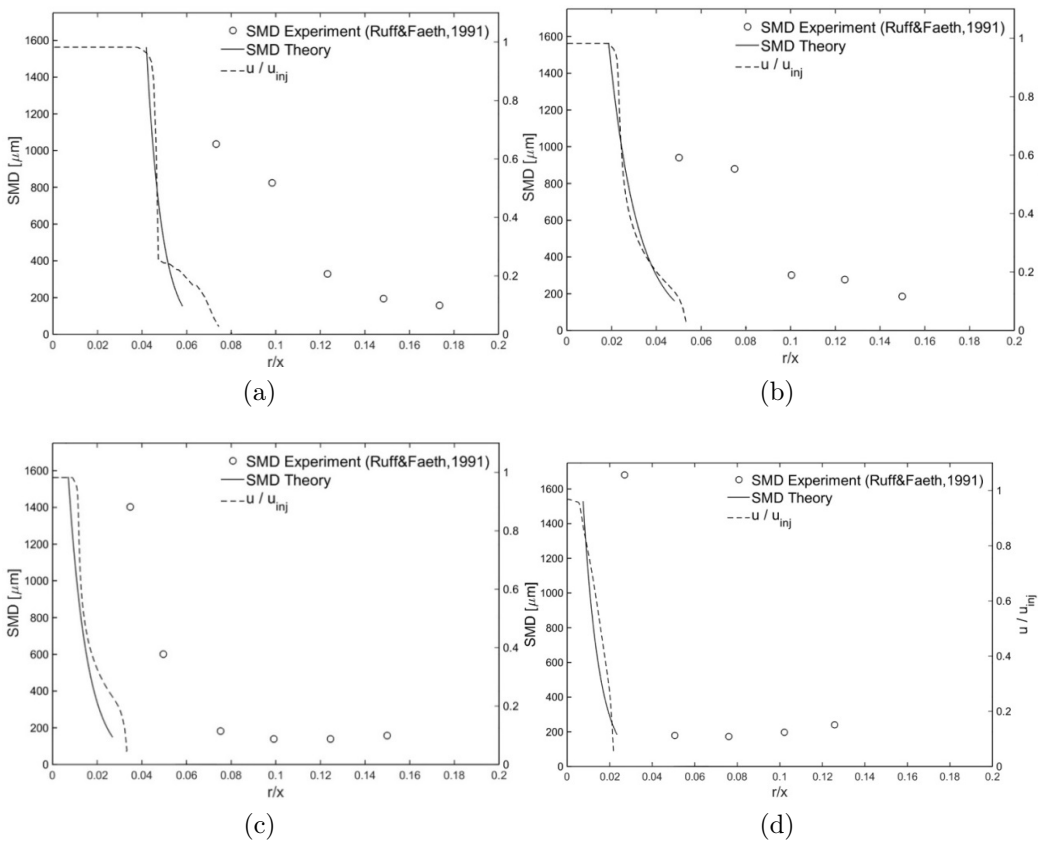

Figure 24. Comparison of the SMD, measured, calculated and also from CFD-generated liquid velocities

CFD is for a liquid jet, with no droplets in the flow. The plots are for x/d = 12.5(a), 25(b), 50(c) and 100(d)

Thus, based on the current and previous research in this laboratory, a robust, physics-based method for inputting the initial drop size and velocities in a CFD setting is feasible. This will involve running a CFD code such as ANSYS/FLUENT for the liquid core. A schematic for this sequence is shown below. The liquid jet in air can be simulated using ANSYS/FLUENT using volume-of-fluid method, and it provides the liquid volume fraction and velocities. Based on this data, we can find the local liquid velocity which we use in quadratic formula, along with an estimate of the mass flux at that point. This mass flux will correspond to the amount of liquid at the given

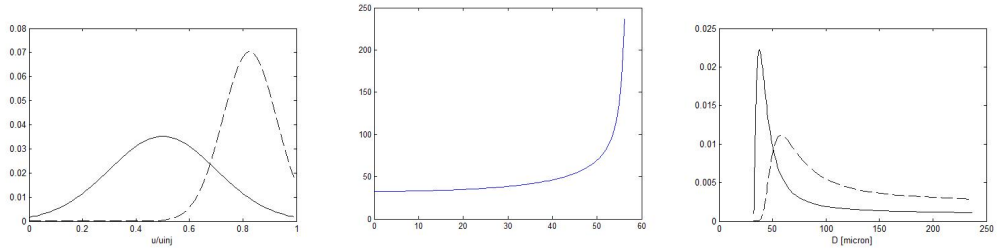

(a) $f(u)$ (b) $D(u)$ from Eq. 6 (c) $g(D)$

Figure 25. Transform from velocity distributions to the drop size distributions via the "quadratic formula"

liquid velocity. As shown in Fig.24, there is a steep decrease in liquid velocity at the periphery of the liquid column so that a range of drop size will be released at the corresponding mass flux. In addition, drop size distributions can be obtained by using the mean and fluctuation velocities, with the latter based on turbulence kinetic energy (k in $k-\epsilon$ models). From the schematic below, and from observations of sprays, most of the mass flux of droplets will occur at the leading tip of the liquid column. Once the droplets are released, their dynamics and thermodynamics can be tracked using particle-in-cell algorithm in ANSYS/FLUENT, or similar. Future work will consist of checking this algorithm results, with experimental data in non-, evaporating, and combusting sprays in various geometries.

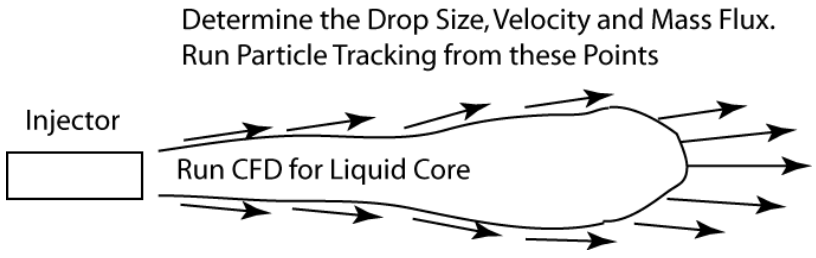

Figure 26. schematic of the application to CFD of spray flows

REFERENCES

[1] Mehran Ahmadi and RW Sellens. "A simplified maximum-entropy-based drop size distribution". In: *Atomization and Sprays* 3.3 (1993).

[2] Hugo Almeida, JMM Sousa, and Mário Costa. "Effect of the liquid injection angle on the atomization of liquid jets in subsonic crossflows". In: *Atomization and Sprays* 24.1 (2014).

[3] Mark R Archambault, Christopher F Edwards, and Robert W MacCormack. "Computation of spray dynamics by moment transport equations II: Application to calculation of a quasi-one-dimensional spray". In: *Atomization and Sprays* 13.1 (2003).

[4] MR Archambault and CF Edwards. *Computation of spray dynamics by direct solution of moment transport equations-inclusion of nonlinear momentum exchange*. Tech. rep. AIR FORCE RESEARCH LAB EDWARDS AFB CA PROPULSION DIRECTORATE WEST, 2000.

[5] E Babinsky and PE Sojka. "Modeling drop size distributions". In: *Progress in energy and combustion science* 28.4 (2002), pp. 303–329.

[6] Julian Becker and Christoph Hassa. "BREAKUP AND ATOMIZATION OF A KEROSENE JET IN CROSSFLOWAT ELEVATED PRESSURE". In: *Atomization and Sprays* 12.1-3 (2002).

[7] Longfei Chen et al. "Formulation of a fuel spray SMD model at atmospheric pressure using Design of Experiments (DoE)". In: *Fuel* 153 (2015), pp. 355–360.

[8] Christophe Dumouchel. "A New Formulation of the Maximum Entropy Formalism to Model Liquid Spray Drop-Size Distribution". In: *Particle & Particle Systems Characterization* 23.6 (2006), pp. 468–479.

[9] Christophe Dumouchel and Stéphane Boyaval. "Use of the maximum entropy formalism to determine drop size distribution characteristics". In: *Particle & Particle Systems Characterization* 16.4 (1999), pp. 177–184.

[10] MM Elkotb. "Fuel atomization for spray modelling". In: *Progress in Energy and Combustion Science* 8.1 (1982), pp. 61–91.

[11] Pontus Eriksson, Raik Orbay, and Jens Klingmann. "Experimental Investigations of a Low Weber Liquid Spray in Air Cross Flow". In: *10th International Conference on Liquid Atomization and Spray Systems*. ICLASS. 2006.

[12] M Eslamian, A Amighi, and N Ashgriz. "Atomization of liquid jet in high-pressure and high-temperature subsonic crossflow". In: *AIAA journal* 52.7 (2014), pp. 1374–1385.

[13] GM Faeth. "Structure and atomization properties of dense turbulent sprays". In: *Symposium (International) on Combustion*. Vol. 23. 1. Elsevier. 1991, pp. 1345–1352.

[14] GM Faeth, L-P Hsiang, and P-K Wu. "Structure and breakup properties of sprays". In: *International Journal of Multiphase Flow* 21 (1995), pp. 99–127.

[15] Stefan Freitag and Christoph Hassa. "Spray characteristics of a kerosene jet in cross flow of air at elevated pressure". In: *Proceedings ILASS-Europe*. 2008.

[16] S Ghosh and JCR Hunt. "Spray jets in a cross-flow". In: *Journal of Fluid Mechanics* 365 (1998), pp. 109–136.

[17] Mikhael Gorokhovski and Marcus Herrmann. "Modeling primary atomization". In: *Annu. Rev. Fluid Mech.* 40 (2008), pp. 343–366.

[18] Marcus Herrmann. "Detailed numerical simulations of the primary atomization of a turbulent liquid jet in crossflow". In: *Journal of Engineering for Gas Turbines and Power* 132.6 (2010), p. 061506.

[19] Robert D Ingebo. "Aerodynamic effect of combustor inlet air pressure on fuel jet atomization". In: *Journal of Propulsion and Power* 1.2 (1985), pp. 137–142.

[20] Sachin Khosla and D Scott Crocker. "CFD modeling of the atomization of plain liquid jets in cross flow for gas turbine applications". In: *ASME Turbo Expo 2004: Power for Land, Sea, and Air*. American Society of Mechanical Engineers. 2004, pp. 797–806.

[21] Kenneth D Kihm, GM Lyn, and SY Son. "Atomization of cross-injecting sprays into convective air stream". In: *Atomization and Sprays* 5.4&5 (1995).

[22] Kyungjin Lee et al. "Primary breakup of turbulent round liquid jets in uniform crossflows". In: *AIAA journal* 45.8 (2007), pp. 1907–1916.

[23] T-W Lee and Keju An. "Quadratic formula for determining the drop size in pressure-atomized sprays with and without swirl". In: *Physics of Fluids* 28.6 (2016), p. 063302.

[24] T-W Lee, JY Lee, and YH Do. "Momentum Effects on the Spray Drop Size, Calculated from the Integral Form of the Conservation Equations". In: *Combustion Science and Technology* 184.3 (2012), pp. 434–443.

[25] T-W Lee and A Mitrovic. "Liquid core structure of pressure-atomized sprays via laser tomographic imaging". In: *Atomization and Sprays* 6.1 (1996).

[26] T-W Lee and Dan Robinson. "Calculation of the drop size distribution and velocities from the integral form of the conservation equations". In: *Combustion Science and Technology* 183.3 (2010), pp. 271–284.

[27] T-W Lee and J-H Ryu. "Analyses of spray break-up mechanisms using the integral form of the conservation equations". In: *Combustion Theory and Modelling* 18.1 (2014), pp. 89–100.

[28] AH Lefebvre. "Atomization and sprays hemisphere publishing corporation". In: *New York* (1989).

[29] Arthur H Lefebvre. "Energy considerations in twin-fluid atomization". In: *ASME 1990 international gas turbine and aeroengine congress and exposition*. American Society of Mechanical Engineers. 1990, V003T06A002–V003T06A002.

[30] David Matthew Less and JA Schetz. "Transient behavior of liquid jets injected normal to a high-velocitygas stream". In: *AIAA journal* 24.12 (1986), pp. 1979–1986.

[31] X Li et al. "Comparison between experiments and predictions based on maximum entropy for sprays from a pressure atomizer". In: *Combustion and Flame* 86.1-2 (1991), pp. 73–89.

[32] Eugene Lubarsky et al. "Spray in crossflow: Dependence on Weber number". In: *Journal of Engineering for Gas Turbines and Power* 132.2 (2010), p. 021501.

[33] Philippe Marmottant and Emmanuel Villermaux. "On spray formation". In: *Journal of fluid mechanics* 498 (2004), pp. 73–111.

[34] CC Miesse. "Correlation of experimental data on the disintegration of liquid jets". In: *Industrial & Engineering Chemistry* 47.9 (1955), pp. 1690–1701.

[35] JC Phillips and PCH Miller. "Field and wind tunnel measurements of the airborne spray volume downwind of single flat-fan nozzles". In: *Journal of Agricultural Engineering Research* 72.2 (1999), pp. 161–170.

[36] Michael Rachner et al. “Modelling of the atomization of a plain liquid fuel jet in crossflow at gas turbine conditions”. In: *Aerospace Science and Technology* 6.7 (2002), pp. 495–506.

[37] William E Ranz. “Some experiments on orifice sprays”. In: *The Canadian Journal of Chemical Engineering* 36.4 (1958), pp. 175–181.

[38] Nicolas Rimbert and Guillaume Castanet. “Liquid atomization out of a full cone pressure swirl nozzle”. In: *arXiv preprint arXiv:1008.2474* (2010).

[39] GA Ruff, LP Bernal, and GM Faeth. “Structure of the near-injector region of nonevaporating pressure-atomized sprays”. In: *Journal of Propulsion and Power* 7.2 (1991), pp. 221–230.

[40] Roland Schmehl. “Advanced modeling of droplet deformation and breakup for CFD analysis of mixture preparation”. In: *Zaragoza* 9.11 (2002).

[41] RW Sellens and TA Brzustowski. “A simplified prediction of droplet velocity distributions in a spray”. In: *Combustion and flame* 65.3 (1986), pp. 273–279.

[42] Maziar Shafaee et al. “SIZE DISTRIBUTION MODELLING OF SECONDARY ATOMIZATION IN SPRAY OF PLAIN-JET AIRBLAST ATOMIZER WITH FINITE STOCHASTIC BREAKUP MODEL”. In: (Apr. 2014).

[43] WA Sirignano and C Mehring. “Review of theory of distortion and disintegration of liquid streams”. In: *Progress in energy and combustion science* 26.4-6 (2000), pp. 609–655.

[44] Jinkwan Song, Charles Cary Cain, and Jong Guen Lee. “Liquid jets in subsonic air crossflow at elevated pressure”. In: *Journal of Engineering for Gas Turbines and Power* 137.4 (2015), p. 041502.

[45] Sandeep D Sovani, Paul E Sojka, and Yudaya R Sivathanu. “Prediction of drop size distributions from first principles: Joint PDF effects”. In: *Atomization and Sprays* 10.6 (2000).

[46] Shankar Subramaniam. “Statistical representation of a spray as a point process”. In: *Physics of Fluids* 12.10 (2000), pp. 2413–2431.

[47] Andreas Tratnig and Günter Brenn. “Drop size spectra in sprays from pressure-swirl atomizers”. In: *International Journal of Multiphase Flow* 36.5 (2010), pp. 349–363.

[48] CWM Van Der Geld and H Vermeer. "Prediction of drop size distributions in sprays using the maximum entropy formalism: the effect of satellite formation". In: *International journal of multiphase flow* 20.2 (1994), pp. 363–381.

[49] Pei-Kuan Wu et al. "Spray structures of liquid jets atomized in subsonic cross-flows". In: *Journal of propulsion and power* 14.2 (1998), pp. 173–182.

[50] P-K Wu, RF Miranda, and GM Faeth. "Effects of initial flow conditions on primary breakup of nonturbulent and turbulent liquid jets". In: (1994).

[51] Li Xianguo and RICHARD S TANKIN0. "Droplet size distribution: A derivation of a Nukiyama-Tanasawa type distribution function". In: *Combustion Science and Technology* 56.1-3 (1987), pp. 65–76.

[52] Sam S Yoon and Stephen D Heister. "A nonlinear atomization model based on a boundary layer instability mechanism". In: *Physics of Fluids* 16.1 (2004), pp. 47–61.

APPENDIX A

APPLICATION FOR DROP SIZE AND VELOCITY DISTRIBUTION

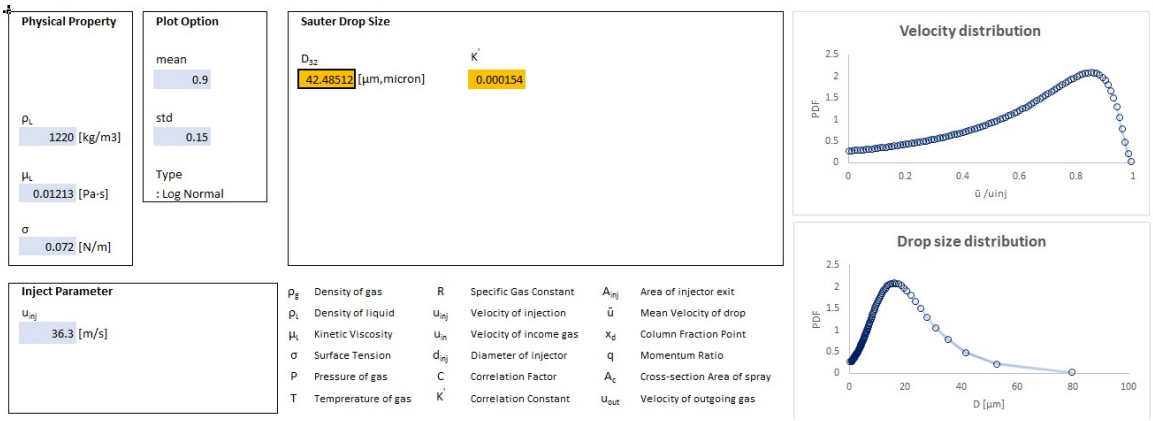

Figure 27. Velocity and Drop size distribution calculator in excel (Log-Normal)

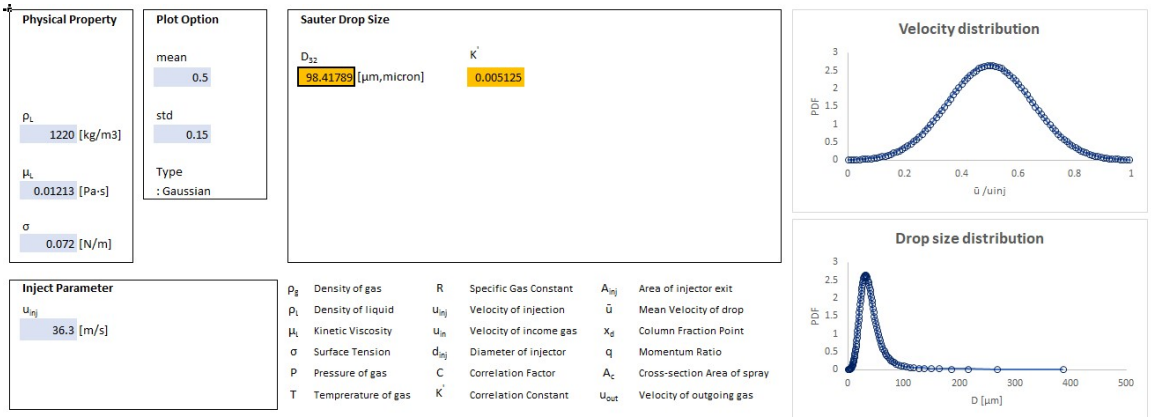

Figure 28. Velocity and Drop size distribution calculator in excel (Gaussian)